SusMat

WILEY

SusMat

REVIEW OPEN ACCESS

Recent Advances of Metal-Organic Frameworks and Derivatives for Rechargeable Aluminum Batteries

Dan-Yang Wang[1] | Hong-Han Choo[1] | Erhai Hu[1] | Jinxuan Song[1] | Afriyanti Sumboja[2] | Ivandini T. Anggraningrum[3] | Anne Zulfia Syahrial[4] | Qingyu Yan[1]

[1]School of Material Science and Engineering, Nanyang Technological University, Singapore, Singapore | [2]Material Science and Engineering Research Group, Faculty of Mechanical and Aerospace Engineering, Institut Teknologi Bandung, Bandung, Indonesia | [3]Department of Chemistry, University of Indonesia, Depok, Indonesia | [4]Metallurgical & Materials Engineering Department, Fakultas Teknik Universitas Indonesia, Kampus UI, Depok, Indonesia

Correspondence: Qingyu Yan (alexyan@ntu.edu.sg)

Received: 20 September 2024 | **Revised:** 21 October 2024 | **Accepted:** 29 October 2024

Funding: Financial support was provided by the ASTAR MTC programmatic project under Grant No. M23L9b0052, Indonesia-NTU Singapore Institute of Research for Sustainability and Innovation (INSPIRASI) under Contract No. 6635/E3/KL.02.02/2023, and Singapore NRF Singapore-China flagship program under Grant No. 023740-00001.

Keywords: aluminum batteries | metal-organic frameworks | performance | structures

ABSTRACT

In light of cost-effectiveness, high volumetric capacity, and abundant supplies on Earth of aluminum metal, the rechargeable aluminum battery (RAB) represents a cutting-edge alternative for energy storage devices. RABs have achieved significant progress as a result of tireless efforts; however, challenges like as expensive ionic liquid electrolytes, a restricted voltage window of aqueous electrolytes, corroded anode, and rapid capacity degradation limit their practical applications. In terms of increasing RAB mileage, electrode materials can be regarded as the foundation of battery performance. Metal-organic frameworks (MOFs), which have customizable topologies, multiple active sites, and various metal centers and ligands, are promising electrode materials. Herein, for the first time, we deliver in detail the recent advancement of MOFs in RABs. The relationship on structure-properties-performance of MOFs is thoroughly discussed. MOF and MOF-derived electrode materials are first summarized. In aluminum sulfur/selenium batteries, MOF can serve as a host to capture the sulfides or selenides. Furthermore, the MOF as catalysts for aluminum-air batteries are provided. Then we focused on the challenges and opportunities that RABs would face in the future, and some prospects are presented. We believe this account will facilitate the exploration of MOFs in RABs and give more inspiration for discovering advanced RABs.

1 | Introduction

In recent years, batteries with elevated energy density have gained recognition as a leading energy technology and a hotly debated research area [1, 2]. Lithium-ion batteries dominate the market due to high energy conversion efficiency and extended lifespan, powering a diverse array of electronics from mobile phones to electric cars [3, 4]. However, questions remain about the expensive cost of metals, limited lithium resources, and poor safety in lithium-ion batteries [5–7]. Therefore, developed state-of-the-art batteries not only focus on high energy density and prolonged lifespan but also on lightweight, pollution-free, and environmentally benignity [8–10].

Aluminum, the third most prevalent element in the Earth's crust, offers a cost-effective alternative (costing only 1/150th the price of lithium metal) to traditional alkali metal batteries [11]. Notably, the aluminum metal electrode has a substantial theoretical

specific capacity of 2979.99 mAh g^{-1}, positioning aluminum-ion batteries at the forefront of next-generation energy storage technologies [12, 13]. Additionally, the three-electron transfer process provides a high energy density, and its smaller ionic radius (0.535 Å) facilitates good electrochemical reaction kinetics [14]. Compared with lithium and sodium, aluminum is less sensitive to air and water, ensuring the high safety of rechargeable aluminum batteries (RABs). Given these advantages, aluminum-ion batteries have garnered significant research interest.

Historically, RABs were first explored in the mid-20th century, though received little attention until the 21st century due to the challenges of finding suitable electrolyte systems and stable cathode materials. Around 2015, research interest increased dramatically and was classified into aqueous and non-aqueous categories [15–17]. Non-aqueous systems typically employ ionic liquid (IL) electrolytes, such as $AlCl_3$-[EMIm]Cl, $Al(OTf)_3$-[BMIm]OTf, which are derived from Al salt and azole function groups [18, 19]. In contrast, aqueous aluminum batteries are low-cost, ecologically benign, and extremely safe [20]. In recent years, RAB research has made tremendous progress [21]. However, challenges remain, such as the elevated cost associated with IL electrolytes and their sensitivity to air and water, whereas aqueous electrolytes have limited voltage windows and hydrogen evolution. There are currently few reports on electrolyte modification engineering. Regardless, continued enhancement of RAB involves investigating electrode materials. Metal oxides, carbon-based, and transition metal-based composites are the most common electrode materials, and they provide excellent operating voltage and rate performance [22–25]. However, the development is limited due to the low capacity between 60 and110 mAh g^{-1} [26]. Accordingly, the investigation of new electrode materials with high energy density, rapid ion migration, and elevated energy conversion rate remains a key priority for the development of RABs.

In the course of developing electrode materials, metal-organic frameworks (MOFs) signify a novel class of alternative electrodes [27–29]. These periodic framework materials provide numerous pores and channels, along with an extensive specific surface area. The metal center in MOFs can consist of either a single metal ion or a metal cluster. Common metal ions include copper, zinc, nickel, and aluminum. Metal clusters are formed by multiple metal ions interconnected through shared oxygen, nitrogen, and other atoms. Organic ligands are molecules that link to metal centers, typically possessing multiple coordination sites (such as nitrogen or oxygen) and flexible carbon chain structures, which enable them to form chemical bonds with the metal center. The coordination of various organic ligands and metal ions endows MOFs with outstanding physical and chemical characteristics and properties. MOFs have been employed as electrode materials in lithium, sodium, and zinc batteries [30–33]. The porous and versatile channel architecture of MOFs facilitates the intercalation and deintercalation of metal ions. Additionally, the metal ions on MOF can change valence during the electrochemical redox process [34, 35], while organic ligands potentially can function as redox-active sites [36–38]. Furthermore, the advantage of adjustable configuration ensures high capacity and cycle stability. Some nanomaterials derived from MOFs, featuring unique framework structures and varied metal compositions, are also promising as electrode materials [39, 40].

MOFs are suitable as electrode materials for RABs. However, research on MOFs for aluminum batteries remains in its early stages, and no exhaustive reviews are currently available. Current MOF reviews report primarily focus on their applications in lithium and zinc batteries, emphasizing material capacity and overall battery performance. Herein, the account aims to fill that gap by providing a comprehensive summary of recent advancements, along with a thorough examination of the interplay between configuration, properties, and performance of MOF in RABs. The pristine MOFs and MOFs-derived materials as electrodes are first overviewed. MOFs as electrolyte components can improve battery performance. In addition, MOFs can act as hosts in aluminum sulfur (Al-S) batteries for capturing sulfides. Then the MOFs or MOFs-derived materials as catalysts in aluminum air (Al-air) batteries are discussed. Finally, some perspectives and future challenges are provided. We anticipate this account will supply more interest and insight for developing MOFs in Al batteries (Figure 1).

2 | Pristine MOFs

MOFs have emerged as a highly promising class of materials for various applications, including cathodes, anodes, or electrolytes in metal-ion batteries. MOF cathodes offer unique advantages, particularly in the context of RABs. Their high porosity and extensive surface area enhance electrode–electrolyte interactions, improving the electrochemical performance of batteries [41–43]. Additionally, The chemical adaptability and tunability of MOFs enable the integration of multi-electron redox sites and linkers, which can yield high specific capacity. Moreover, smaller MOF particles can enhance electrochemical stability by mitigating swelling, as the interparticle spaces act as volumetric buffers during charge–discharge cycles. This stability is essential for ensuring sustained battery performance over extended periods [44–46]. MOFs also show promise for applications requiring augmented flexibility, improved transparency, and elevated charge carrier mobility, opening up new avenues for flexible and wearable electronics.

The structure and permeable channels of MOFs can facilitate a distinctive pathway for ion transport, significantly enhancing interface stability and cycling performance in batteries. The first row of transition metal ions (such as Fe^{II}, Co^{II}, Ni^{II}, and Cu^{II}) provide strong coordination ability with ligands, as partially filled d-orbitals can offer sufficient electron vacancies to facilitate electron exchange during electrochemistry reactions [47, 48]. A major challenge with organic electrode materials is their tendency to dissolve in electrolytes, leading to poor cycling stability. MOFs have physical or chemical confinement effects, serving as hosts to prevent the dissolution of organic electrodes [49, 50]. Lu et al. described a one-pot synthesis method for polyimide (PI) combined with MOFs (PI/MOF) to serve as cathode materials in RABs (Figure 2A) [51]. Intense interactions between N-H···O-C hydrogen bonds facilitate the connection of the C-O parts of imine moiety to the N-H group of 2-methylimidazole. Porous MOFs can efficiently avoid the aggregation of PI and minimize its dissolution in IL electrolytes, thereby enhancing overall stability. PI/MOF as cathode provides the discharge capacity of 83 mAh g^{-1} at 1000 mA g^{-1} with a long cycle life of 1800 cycles and a low decay of 0.0067% per cycle (Figure 2B). Xiong et al. reported a

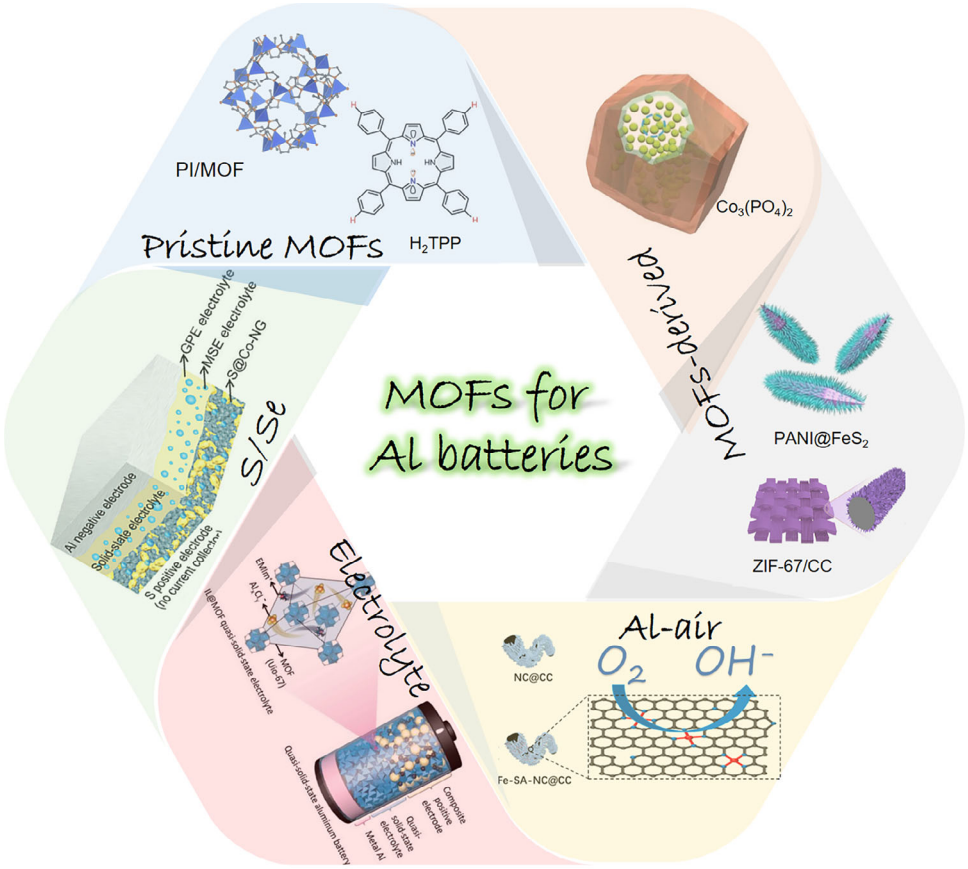

FIGURE 1 | Schematic of summary of different uses of metal-organic frameworks (MOFs) in rechargeable aluminum battery (RAB).

stretchable, fiber-shaped aqueous aluminum-ion battery comprising a manganese hexacyanoferrate cathode, a graphene oxide-modified MoO_3 anode, and a hydrogel electrolyte [52]. The battery exhibits excellent stretchability and, through a rocking-chair storage mechanism, delivers a high specific capacity of 42 mAh cm^{-3}. Moreover, it maintains a capacity retention rate of 91.6% after 100 cycles.

Besides serving as host materials, MOFs can function as electrode materials for RABs, attributed to their functional structure that allows for electron gain and loss. Jiao et al. reported that π-conjugated organic porphyrin molecules can be employed directly as cathode materials for RABs [53]. Porphyrins exhibit narrow energy gaps between the highest occupied molecular orbital (HOMO) and the lowest occupied molecular orbital (LUMO), resulting in elevated electrochemistry activity and rapid electron transfer. 5,10,15,20-tetraphenyl porphyrin (H_2TPP) and 5,10,15,20-tetrakis(4-carboxyphenyl) porphyrin (H_2TCPP) were acted as cathode materials with the same 18 π electron system (Figure 2C). The CV profile of the H_2TPP reveals two distinct pairs of peaks occurring at 1.7/1.65 V and 2.0/1.93 V, respectively; however, the redox signal of H_2TCPP is less pronounced, primarily due to the influence of carboxyl with electron-withdrawing, which leads to a reduction in electron cloud density of conjugated systems and inhibit the coordination reaction with $AlCl^{2+}$. The active site of the H_2TPP molecule resides on the nitrogen atom with lone pair electrons, facilitating its interaction with Al ions. The Al-H_2TPP reveals a first discharge capacity of 84.8 mAh g^{-1}, stable cycling over 5000 cycles, and Coulombic efficiency of around 98% (Figure 2D). Subsequently, they reported a Cu-based MOF cathode material for RABs [54]. The bipolar ligands in two-dimensional (2D) Cu-based MOFs can achieve cyclic storage of $AlCl_4^-$ anions and $AlCl^{2+}$ cations during the charging and discharging state (Figure 3A). The 2D Cu-based MOF microchips are arranged in AB packaging, forming a spatial group of I4/mmm configuration with an interlayer distance of ≈1.3 nm, which offers sufficient capacity to house sizable chloroaluminate ions. This distinctive ultra-thin microstructure creates additional open channels that enhance electrolyte permeation and facilitate ion diffusion, thus exposing more active sites. All anions and cations participate in the entire redox process. During the initial charging state, the organic ligands in the MOF are oxidized from 18 π electrons to 16 π electrons, accompanied by the insertion of $AlCl_4^-$ anions (Figure 3C). Upon discharge, the organic ligand gains electrons and is reduced to 18 π electrons as $AlCl^{4-}$ is released (from II to I). The subsequent reduction from 18 π to 20 π electrons causes the $AlCl^{2+}$ cation to insert into the MOF (from I to III), followed by a reduction of Cu^{II} to Cu^{I}, with $AlCl^{2+}$ adsorbed on the Cu site (from III to IV). The cathode can exhibit the specific capacity of 184 mAh g^{-1}. Even after 1000 cycles, it maintains a stable high capacity of 155 mAh g^{-1} (Figure 3B).

Metal-organic polymers (MOPs) have surfaced as exceptionally versatile organic materials with multifunctional properties, characterized by unique framework structures, high stability, and redox activity, making them highly suitable as electrode materials for RABs. Pakulski et al. synthesized two new MOPs by coordinating the redox-active tetraminobenzoquinone (TABQ)

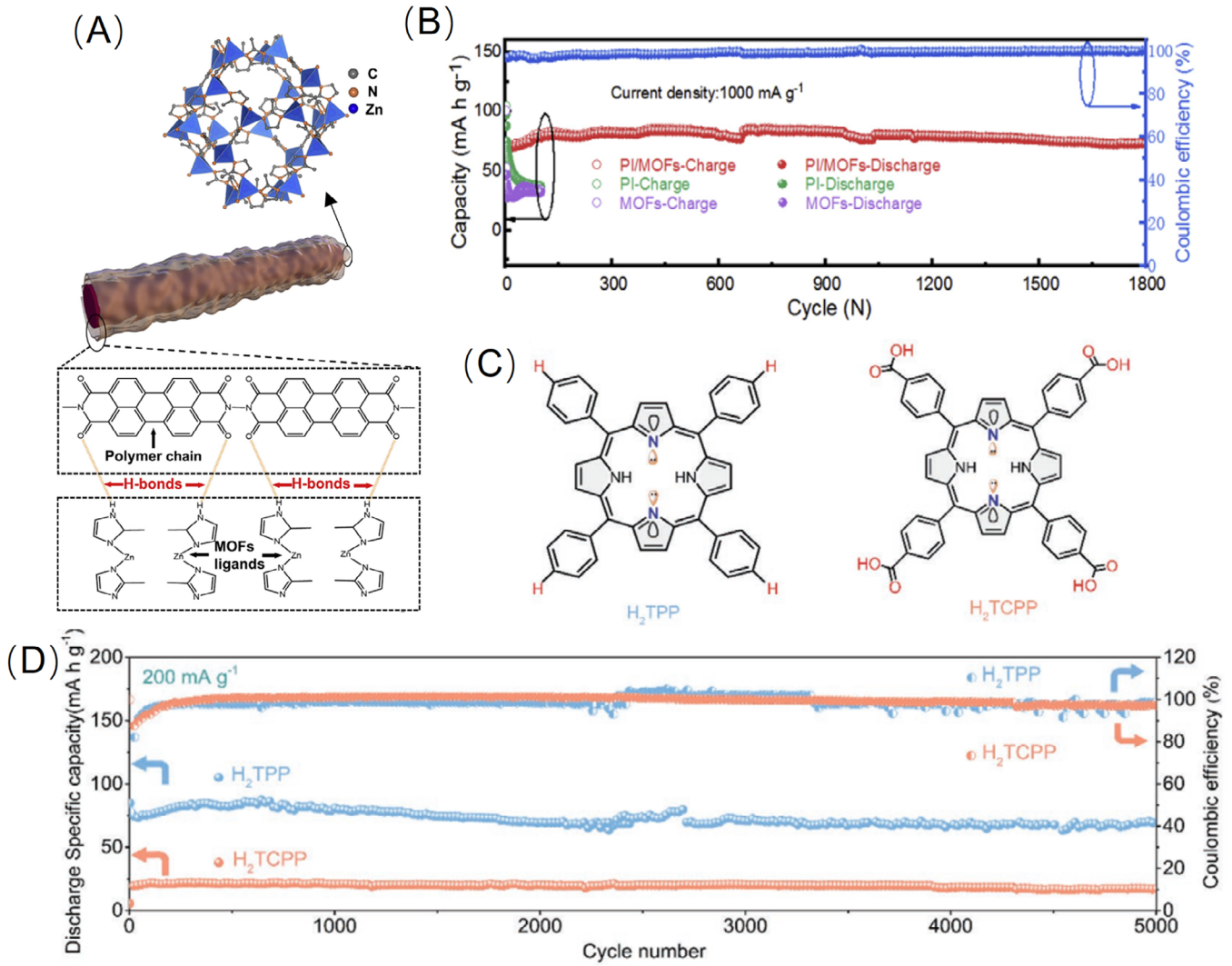

FIGURE 2 | (A) Illustration of H bonds in polyimide (PI)/MOFs configuration. (B) The cycling performance of PI, MOFs, and PI/MOFs hybrid. Reproduced with permission: Copyright 2020, Elsevier [51]. (C) Molecular structure of 5,10,15,20-tetraphenyl porphyrin (H_2TPP) and 5,10,15,20-tetrakis(4-carboxyphenyl) porphyrin (H_2TCPP). (D) The battery performance of H_2TPP and H_2TCPP. Reproduced with permission: Copyright 2021, Wiley-VCH [53].

monomer with divalent metal ions (Zn^{2+} and Cu^{2+}) [55]. The coordination of nitrogen atoms with Zn^{2+} or Cu^{2+} leads to the redistribution of electrons on nitrogen atoms (Figure 3D). The hydrogen bond of the oxygen atom of carbonyl benzoate and the hydrogen atom of imine contributes to the formation of a resilient 2D layered configuration. Moreover, Zn^{2+} and Cu^{2+} form bonds with TABQ by coordinating with the four N atoms of two TABQs, leading to a uniform three-dimensional (3D) network structure. The pore size shows that Cu-TABQ is mainly microporous with the pore diameter of 3.72 nm, while Zn-TABQ is predominantly mesoporous and macroporous with an average pore size of 28.95 nm. The ion conductivity of Zn-TABQ reaches 0.12 S m^{-1}. This value is roughly 40% greater, compared to that of the Cu-TABQ (0.08 S m^{-1}), thus promoting stable battery performance. Zn-TABQ presents a high capacity of 198 mAh g^{-1} at 0.05 A g^{-1} and high cycling stability with a retention of 92% over 5000 cycles (Figure 3E).

With a high theoretical capacity (1040 mAh cm^{-3}) under conversion reaction mechanisms, iodine is a promising cathode material; nevertheless, its implementation is impeded by challenges such as limited conductivity, inadequate thermal stability, and high solubility. Using porous conductive structures to physically adsorb and chemically combine iodine can solve these problems. Yang et al. reported the encapsulation of approximately 30 wt% iodine in nitrogen-doped microporous carbon polyhedra derived from MOF, denoted as I_2@ZIF-8-C (Figure 3F), that exhibits a rhombic dodecahedral shape [56]. After iodine is introduced into the porous, no intrinsic particles are detected external to the ZIF-8-C framework, demonstrating the effective confinement of iodine within the conductive carbon. Nitrogen on conductive carbon has strong chemical adsorption to iodine. Furthermore, the robust interaction of ZnO and iodine is beneficial for inhibiting the dissolution of polyiodides. It is noteworthy that a "water-in-salt" electrolyte (WISE) is employed, consisting of a combination of 1 M $AlCl_3$ and 9 M lithium bis(trifluoromethanesulfonyl)imide (LiTFSI). I_2@ZIF-8-C displays three separate discharge plateaus at 0.8, 1.3, and 1.6 V (Figure 3G), corresponding to the conversion of I_2 to AlI_3. Importantly, the main reaction involves reversible redox of I^{3-} and I^{5-} between I^- and I_2, that is, $I_2 \leftrightarrow I^{5-} \leftrightarrow I^{3-} \leftrightarrow I^-$

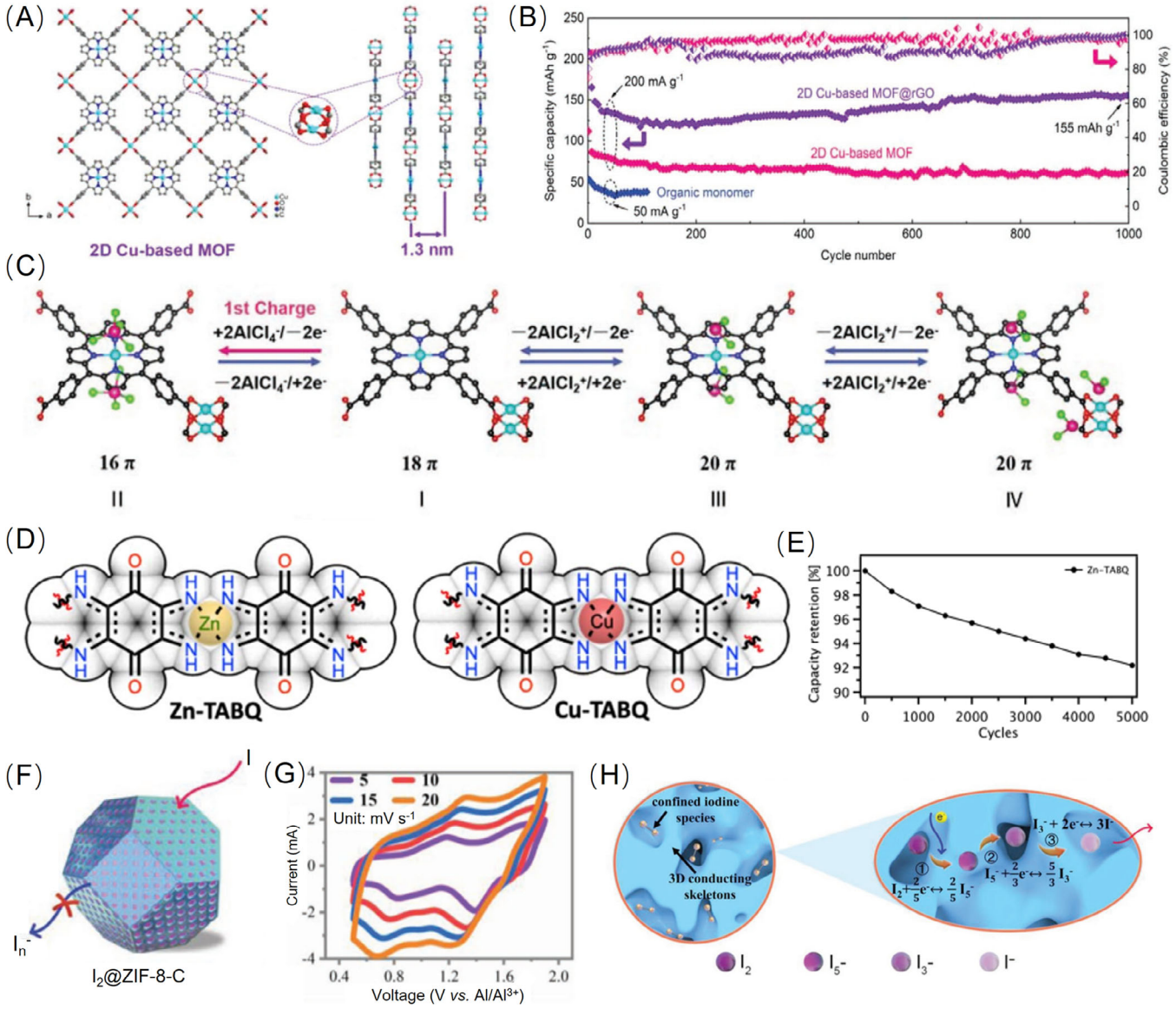

FIGURE 3 | (A) Illustration of two-dimensional (2D) Cu-based MOF. (B) The battery performance at 200 mA g^{-1} of different MOF composites. (C) Illustration of the charge storage process in 2D Cu-based MOFs Reproduced with permission: Copyright 2022, Wiley-VCH [54]. (D) The structures of Zn-TABQ and Cu-TABQ MOPs. (E) Cycling performance of Zn-TABQ. Reproduced with permission: Copyright 2024, Royal Society of Chemistry [55]. (F) Configuration of I_2@ZIF-8-C. (G) CV profiles of aqueous Al//I_2@ZIF-8-C battery with different scan rates. (H) The schematic representation of the three-step electrochemical process of the I_2@ZIF-8-C electrode. Reproduced with permission: Copyright 2021, Wiley-VCH [56].

(Figure 3H). I_2@ZIF-8-C shows the initial discharge capacity of 259 mAh g^{-1} and retains 162.0 mAh g^{-1} over 150 cycles. Even at a high current density of 8 A g^{-1}, the cell can obtain 102.6 mAh g^{-1}.

3 | MOFs-Derived Composites

Unlike conventional porous nanostructured materials, MOF-based nanostructures feature precisely controllable and uniform porosity, well-ordered crystalline structures, a high density of metal active sites, excellent chemical stability, a substantial surface area, and sustained durability over time [57, 58]. These attributes render MOF derivatives highly promising for applications in energy storage systems, offering versatile functionalities for electrode materials in rechargeable batteries [59–61].

Xiao et al. researched adding polyvinyl (PVP) iodine and pre-treated MWCNTs to the mixture of ZIF-67, followed by calcination resulting in the formation of Co_3O_4@MWCNTs. Furthermore, with the IL ([EMIm]Al_xCl_y) electrolyte [62], the Co_3O_4@MWCNTs cathode exhibits a high initial capacity of approximately 266.3 mAh g^{-1} with the commendable cycle of 125 mAh g^{-1} over 150 cycles (Figure 4A). The electrochemical process is identified as the reversible valence change of Co from Co_3O_4 to Co^0. Compared to the performance of pure Co_3O_4 and MOF-derived Co_3O_4, the addition of MWCNTs significantly enhances the conductivity, stability, and capacity. Zhang et al. used a novel strategy to encapsulate metal oxide nanoparticles in reduced graphene oxide (rGO). These oxide nanoparticles are derived from MOF via a facile self-assembly process in aqueous solutions, followed by annealing in an argon atmosphere (Figure 4B).

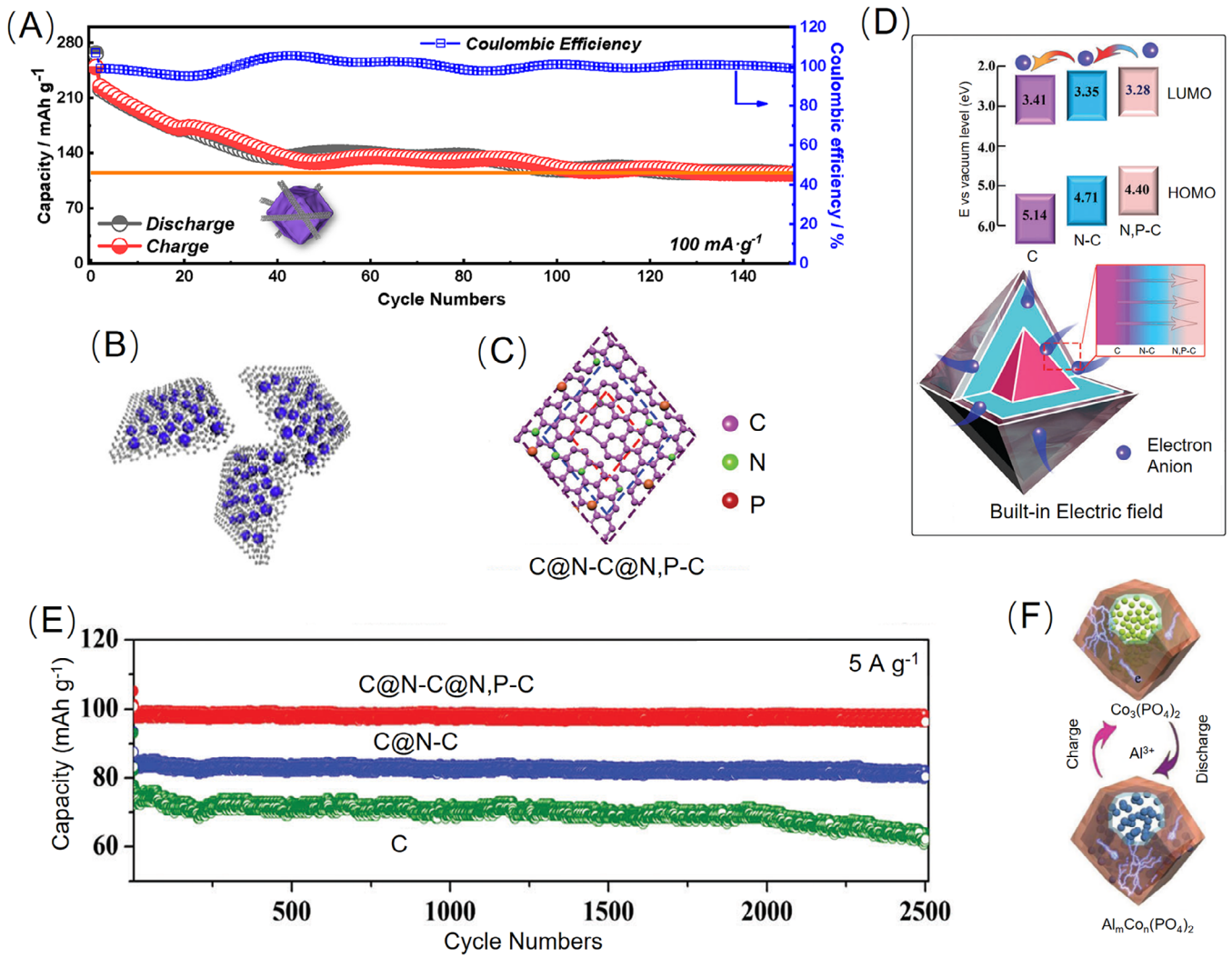

FIGURE 4 | (A) Cycling performance of MOF-derived Co composites (B) Metal-oxide NPs@rGO. Reproduced with permission: Copyright 2019, American Chemical Society [62]. (C) C@N-C@N, P-C octahedron heterostructures. (D) The energy levels for the C, N-C, and N,P-C samples, along with the built-in electric field arising from the charge distribution. (E) Cycling performance of AIBs based on different composite materials. Reproduced with permission: Copyright 2018, Royal Society of Chemistry [64]. (F) The electrochemical redox process of $Co_3(PO_4)_2$. Reproduced with permission: Copyright 2019, Wiley-VCH [65].

Several metal oxides were tried, such as Co_3O_4, Fe_2O_3, and $CoFe_2O_4$, all of which demonstrated high electrochemical activity toward Al^- ion storage in pouch cells with the ionic-liquid electrolyte when encapsulated by rGO [63]. Among the three types of composites, Co_3O_4@rGO exhibits a high initial capacity of 234 mAh g^{-1} and sustains a 168 mAh g^{-1} after 500 cycles at 200 mA g^{-1}.

Zr-MOFs and melamine phosphate are employed as initial substances to form gradient nitrogen and nitrogen doping in porous carbon octahedra (Figure 4C) [64]. This doping creates a built-in electric field that enhances charge transfer and improves the kinetics of $AlCl_4^-$ anions in RABs. During the charging process, the inherent electrostatic forces facilitate the migration of adsorbed $AlCl_4^-$ anions and electrostatic anions from the shell to core, which results in an enhancement of capacity (Figure 4D). The resulting heterostructure serves as cathode material and provides the capacity of 98 mAh g^{-1} at 5 A g^{-1} after 2500 cycles (Figure 4E). Furthermore, the ZIF-67-derived $Co_3(PO_4)_2$@C composites were prepared as electrode material for RAB, featuring a large interplanar spacing, fast ionic mobility, and enhanced electrical conductivity [65]. The carbon shell and porous configuration mitigate variations in volume while preserving the original structural integrity (Figure 4F). As a result, the $Co_3(PO_4)_2$@C hybrid can supply a high reversible capacity of 151 mAh g^{-1} at 2 A g^{-1} after 500 cycles with a capacity decay of 0.02% and Coulombic efficiency beyond 99%. The composites also exhibit exceptionally high rate expression, retaining 111 mAh g^{-1} at 6 A g^{-1}.

Cobalt sulfides, such as $Co_{1-x}S$, CoS, CoS_2, Co_3S_4, and Co_9S_8, are used as electrode materials attributed to their unique catalytic and electrochemistry properties, which can be synthesized using MOF precursors. For example, nano ZIF-67 dispersed on a carbon matrix with a regular hexagonal shape of about 200 nm to prepare CoS1.097@C as a cathode material for RAB (Figure 5A) [66]. The formed $Co_{1.097}S$ has a defect structure containing vacancies, which is beneficial for the insertion/extraction of

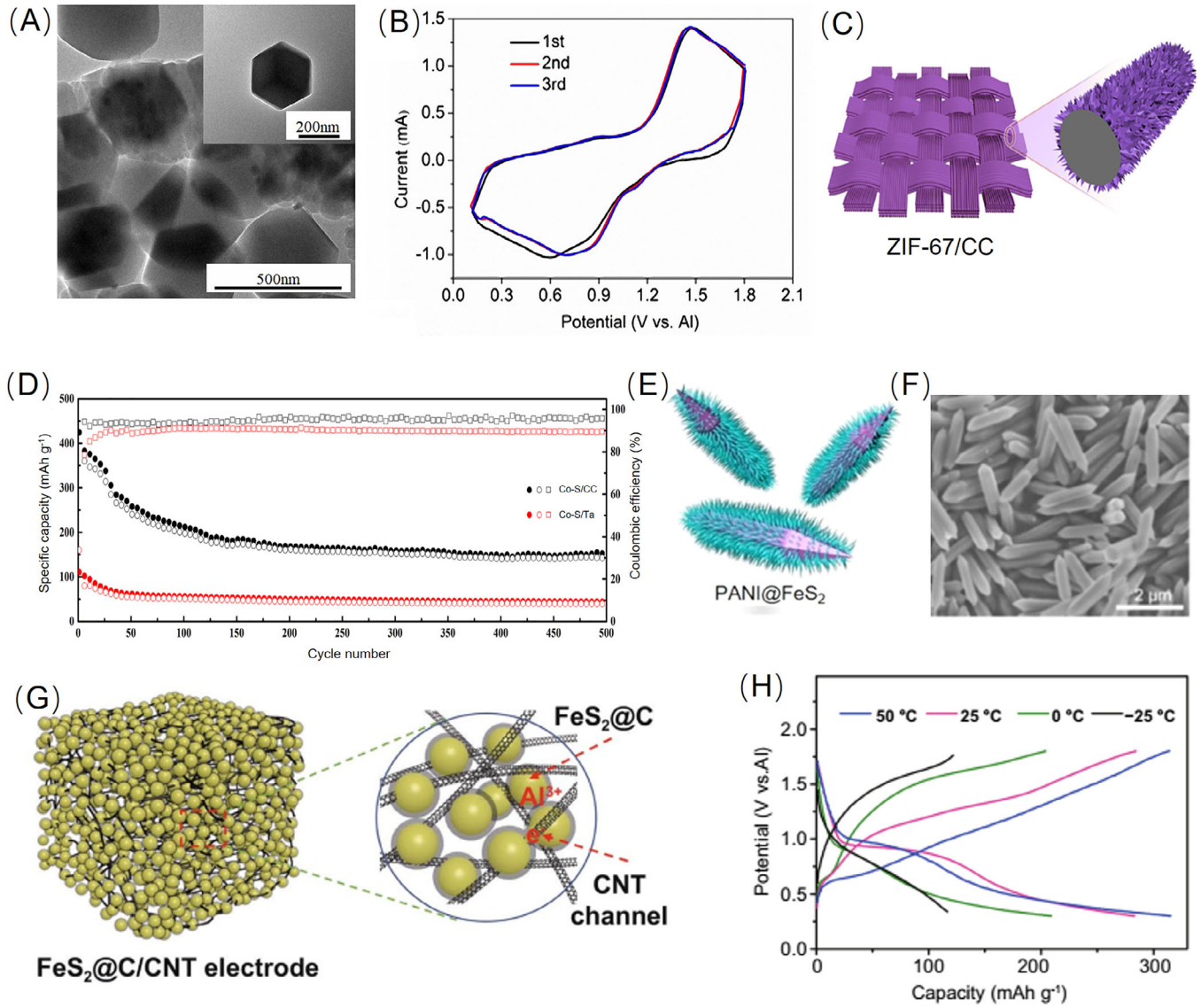

FIGURE 5 | (A) TEM images of nano ZIF-67. (B) CV profiles of the CoS1.097@C cathode. Reproduced with permission: Copyright 2021, Elsevier [66]. (C) Composite of ZIF-67 and carbon cloth. (D) Cycling performance of Co-S/CC batteries. Reproduced with permission: Copyright 2022, Elsevier [67]. (E) The PANI@FeS_2 hybrid materials. (F) SEM image of the MIL-88A precursor. Reproduced with permission: Copyright 2023, Royal Society of Chemistry [69]. (G) The self-standing, binder-free FeS_2@C/CNT features an interpenetrating network configuration. (H) Voltage profiles of the FeS_2@C/CNT and FeS_2/C electrode. Reproduced with permission: Copyright 2021, Springer [70].

Al^{3+}. This is reflected in the CV profile, where the reduction and oxidation signals of $CoS_{1.097}$@C are located at 0.7 and 1.5 V (Figure 5B). $CoS_{1.097}$@C can deliver the specific capacity of 80 mAh g^{-1} at the current density of 100 mA g^{-1} after 500 cycles. Additionally, Jiao et al. developed self-supporting Co-S nanosheets with dual active sites on carbon cloth fibers (Co-S/CC) utilizing ZIF-67 as the precursor [67]. The 3D Co-S/CC presents superior conductivity, extensive surface area, and porous configuration, thereby enhancing the utilization of active substances (Figure 5C). The self-supporting structure eliminates the need for binders and conductive agents, thereby reducing the inactive mass of the electrode. Compared to traditional melt diffusion and heat-induced vulcanization, this more environmentally friendly preparation method offers significant advantages. During charge and discharge cycles, the valence states of Co and S in the Co-S phase fluctuate, with the discharge voltage of Co and S reaching 1.1 V versus Al/$AlCl^{4-}$. Furthermore, Co-S nanosheets are uniformly dispersed over the surface of CC. Notably, the Co and S components in the Co-S/CC cathodes contribute significantly to achieving high capacity. The Co-S/CC cathode demonstrates a first discharge capacity of 383.4 mAh g^{-1}, retaining a high capacity of 156.9 mAh g^{-1} after 500 cycles, with a Coulombic efficiency exceeding 95.8% (Figure 5D).

Non-carbon-based MOFs, though less common, show performance comparable with carbon-based MOFs such as ZIF 67. Han et al. focus on a high-performance cathode material, $Cu_{1.95}S$@CoS_2, which offers a long cycle life and high-temperature tolerance [68]. This MOF-derived octahedral $Cu_{1.95}S$@CoS_2 composite, where CoS_2 nanoparticles grow in situ on $Cu_{1.95}S$. The high surface area and multiple redox sites for interaction with $AlCl_4^-$ enhance battery performance. The $Cu_{1.95}S$@CoS_2 cathode

upholds the capacity of 136.6 mAh g^{-1} after 200 cycles at room temperature and 122.4 mA g^{-1} at -10°C.

FeS_2, known for reserves, low prices, and high conductivity, can theoretically store metal ions. However, FeS_2 exhibits significant volume exchange during charge and discharge, resulting in structural degradation during long-term cycling. To address this issue, MOF-derived nanowire microrod polyaniline hybrid materials PANI@FeS_2 were prepared [69]. PANI nanowires with mechanical flexibility can enhance electron transfer during electrochemical reactions (Figure 5E). Utilizing the MIL-88A as the precursor, PANI nanowires, measuring 100–200 nm in length and diameter of 20–50 nm, were grown in situ via polymerization on FeS_2 (Figure 5F). The mass fractions of FeS_2 and PANI in PANI@FeS_2 are 61.8% and 38.2%, respectively. The electrochemical redox process entails the evolution from FeS_2 to FeS. PANI@FeS_2 as cathode can deliver the initial discharge capacity of 152.8 mAh g^{-1} and provide 193.4 mAh g^{-1} after 500 cycles. Additionally, Wang et al. reported an all-climate aluminum ion battery utilizing the MOF-derived FeS_2@C/CNT as electrode material [70]. The FeS_2 particles are homogeneously dispersed within the carbon nanotubes, forming a thickness of 100 µm. As etching time increases, the structure of the original Fe-MOF progressively degrades, resulting in the formation of a yolk-shell architecture. The performance enhancement of FeS_2@C/CNT is mainly attributed to the enhancement of redox sites within the carbon coating, conductive matrix, and egg yolk-shell architecture (Figure 5G). The binder-free, self-supporting design minimizes the decomposition and side reactions of active materials, greatly enhancing electrochemical stability at ambient temperature. The CV curves exhibit the redox signal at 1.3 and 0.7 V, mainly involving the reaction between FeS_2 and FeS. The FeS_2@C/CNT shows the specific capacity of 286 mAh g^{-1} at 100 mA g^{-1}. The cell can retain 80 mAh g^{-1} after 2000 cycles. Most studies on AIBs concentrate on electrochemical performance at room or elevated temperatures. Remarkably, the cell operates effectively from −25°C to 50°C, maintaining a specific capacity of 117 mAh g^{-1} even at -25°C (Figure 5H).

Selenium (Se), abundant in the crust and superior in conductivity to S, is utilized as a cathode material with a theoretical specific capacity of 675 mAh g^{-1} [71–73]. MOF-derived material can be combined with Se to obtain high-performance electrodes. Hong et al. synthesized Co-MOFs using a 3D ordered macroporous scaffold (SOM ZIF-67), achieved through precise regulation of the nucleation process [74]. The SOM ZIF-67 was combined with Se powder as a precursor and heat treated in an Ar atmosphere to prepare 3D cobalt selenide@carbon (3DOM $CoSe_2$@C), achieving simultaneous carbonization and selenization (Figure 6A). After calcination, the tetrahedral configuration and ordered macroporous framework were well preserved. The interconnected macropores with extensive channels allow to accelerate the transmission of macromolecules (Figure 6B). The extensive surface area of $CoSe_2$ nanoparticles within a conductive 3D framework enhances the transportation of large $Al_xCl_y^-$ species and facilitates electrolyte infiltration. As the cathode, 3D $CoSe_2$@C presents the discharge capacity of 400 mAh g^{-1} at the current density of 1.0 A g^{-1} (Figure 6C). The CV profile reveals two reduction peaks at 0.9 and 1.8 V, as well as two oxidation signals at 1.0 and 2.1 V. The cell maintains a specific capacity of 125 mAh g^{-1} after 1000 cycles.

Another type of improvement is to prepare the cobalt selenide (CoSe@C) composite from MOF with the encapsulation strategy through a heat treatment process [75]. The encapsulation of cobalt selenide can enhance the conductivity, ion diffusion, and configuration integrity of ZIF-67. The fabrication procedure entails the selenization of cobalt-based ZIF-67, subsequently subjected to annealing to produce the CoSe@C composite material. CoSe@C as cathode displays a remarkable specific capacity of 427 mAh g^{-1} and high energy density of 424 Wh kg^{-1}.

Additionally, Wu et al. used the MIL-88A@Fe-Co hydroxide yolk-shell nano-tubes (YSNTs) as the incorporating substances of Se providing a large space for the embedding Se compounds (Figure 6D) [76]. At 500°C, the structure of Fe-Co hydroxide nanosheets is disrupted, leading to Co^{2+} participating in the reaction between Fe and Se. The generated $FeSe_2$ and FeCoSe are embedded in the gaps of hydroxide nanosheets, forming the cathode materials. Moreover, the CV curves provide a reduction peak of approximately 1.6 V and an oxidation peak of nearly 2.1 V (Figure 6E), reflecting the redox process involves the conversion of Fe^{2+} to Fe^{3+} and Se_2^{2-} to Se_2^{2+}. The YSNT@Se cell presents the initial discharge capacity of 292.21 mAh g^{-1} and retains 79.85% over 500 cycles. Furthermore, Cu_2Se nanoparticles were embedded in a 3D porous structure derived from HKUST-1 to serve as cathode materials for RABs [77]. HKUST-1 displays a consistent polyhedral configuration with a typical particle size of 500 nm, and the Cu_2Se@C composite retains the polyhedral morphology of the original HKUST-1 precursor (Figure 6F). This structure possesses rich porosity, facilitating conducive to electrolyte permeation and ion or electron diffusion, thereby improving reaction kinetics. The Cu_2Se@C cathode presents a discharge voltage of approximately 1.8 V. The reduction reaction involves the process of Cu^+ reduction to Cu and Cu-Al alloy, while the oxidation matches the regeneration of Cu_2Se. The cathode delivers the first discharge capacity of 241.9 mAh g^{-1} at 800 mA g^{-1} and maintains 64 mAh g^{-1} after 200 cycles (Figure 6G).

In addition to cobalt selenide, Zhang et al. prepared $CoTe_2$ nanoparticles derived from MOF@nitrogen-doped porous polyhedral composition ($CoTe_2$@N-PC) (Figure 7A) [78]. The synthesis process involving a simple carbonization/tellurization treatment of ZIF 67 nanocrystals and allows the $CoTe_2$@N-PC composites to retain the precursor morphology while acquiring a mesoporous carbon matrix. Heteroatom doping, such as with nitrogen and oxygen, has been demonstrated to optimize the electronic structure and significantly enhance conductivity. Uniformly sized $CoTe_2$ nanoparticles are densely encapsulated within a carbon matrix, effectively preventing direct contact with the electrolyte. The $CoTe_2$@N-PC supplies an exceptional first capacity of 635.8 mAh g^{-1} at 200 mA g^{-1}, operating within high cut-off voltages of 0.5-2.3 V. During the charging process, Te undergoes deep oxidation, transitioning from Te^{2-} to Te^0, then to Te^{2+}, and finally to Te^{4+}. After 200 cycles, the capacity remains remarkably high at 168.6 mAh g^{-1}, with overall Coulombic efficiency exceeding 90% (Figure 7B). Using HKUST-1, Qin et al. synthesized CuTe@porous carbon composites, through a carbonization/tellurization strategy [79]. The blue crystal HKUST-1 framework is composed of dimeric metal units, which are linked by $Cu(NO_3)_2 \cdot 3H_2O$ and trimesic acid (H_3BTC) (Figure 7C). It can maintain the precursor's morphology and form a porous configuration that enhances diffusion transport and

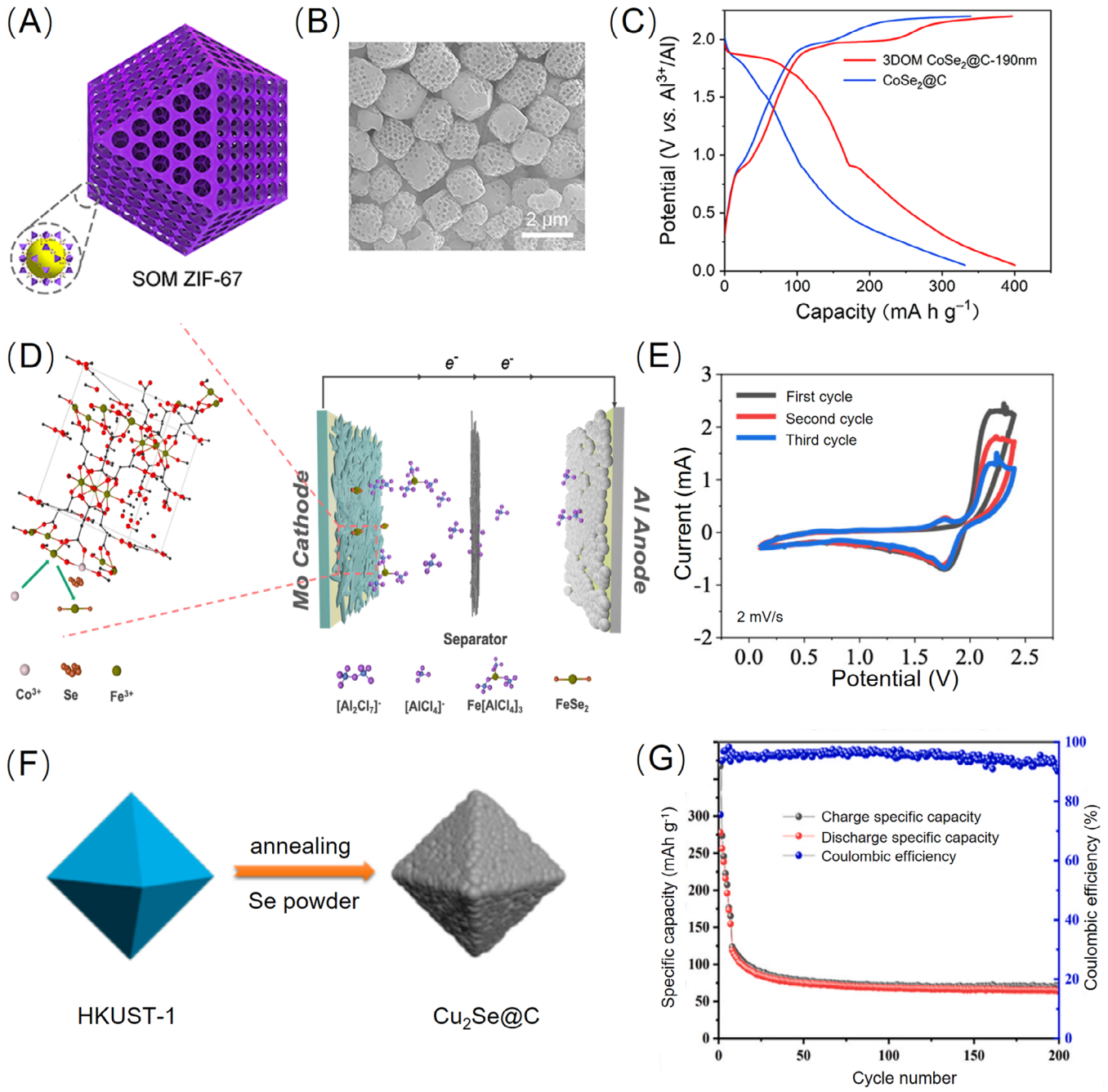

FIGURE 6 | (A) Configuration of SOM ZIF-67. (B) Morphological and structural characterization of SOM ZIF-67. (C) Charge–discharge curves of 3DOM and $CoSe_2$@C. Reproduced with permission: Copyright 2019, American Chemical Society [74]. (D) Illustration of the Al-YSNT@Se battery for charge process. (E) CV curves of Al-YSNT@Se battery. Reproduced with permission: Copyright 2021, American Chemical Society [76]. (F) The schematic depicting the fabrication procedure Cu_2Se@C. (G) Battery performance of Al/Cu_2Se@C battery. Reproduced with permission: Copyright 2023, Elsevier [77].

electrochemical activity. The CuTe@C cathodes exhibit a high first specific capacity of 556.3 mAh g^{-1} at 200 mA g^{-1}, with a distinct voltage plateau around 1.3 V. Moreover, the reaction mechanism involves the inclusion/exclusion of $AlCl^{4-}$ ions.

The mixture composite of iron phosphide (FeP) and cobalt phosphide (CoP) was prepared using a pyramidal MIL-88A, which can accommodate volume expansion and provide multiple active sites [80]. The synthesis process entails the in situ growth of CoP nanosheets onto FeP nanorods (Figure 7D). The FeP@CoP shows a large capacity of 168 mA g^{-1} and high stability, ascribed to the unique structure, where CoP nanosheets support the volume expansion of FeP and FeP nanorods provide a strong backing for the CoP nanosheets. The reaction kinetics of a graphite cathode in urea-based ILs at room temperature are suboptimal, hindering the efficient movement of ions. Wang et al. synthesized MOF-derived hierarchical porous carbon octahedrons (HPCO) characterized by a porous architecture and a durable graphitic (Figure 7E) [81]. The HPCO exhibits enhanced rate performance and cycling stability in comparison to conventional graphite

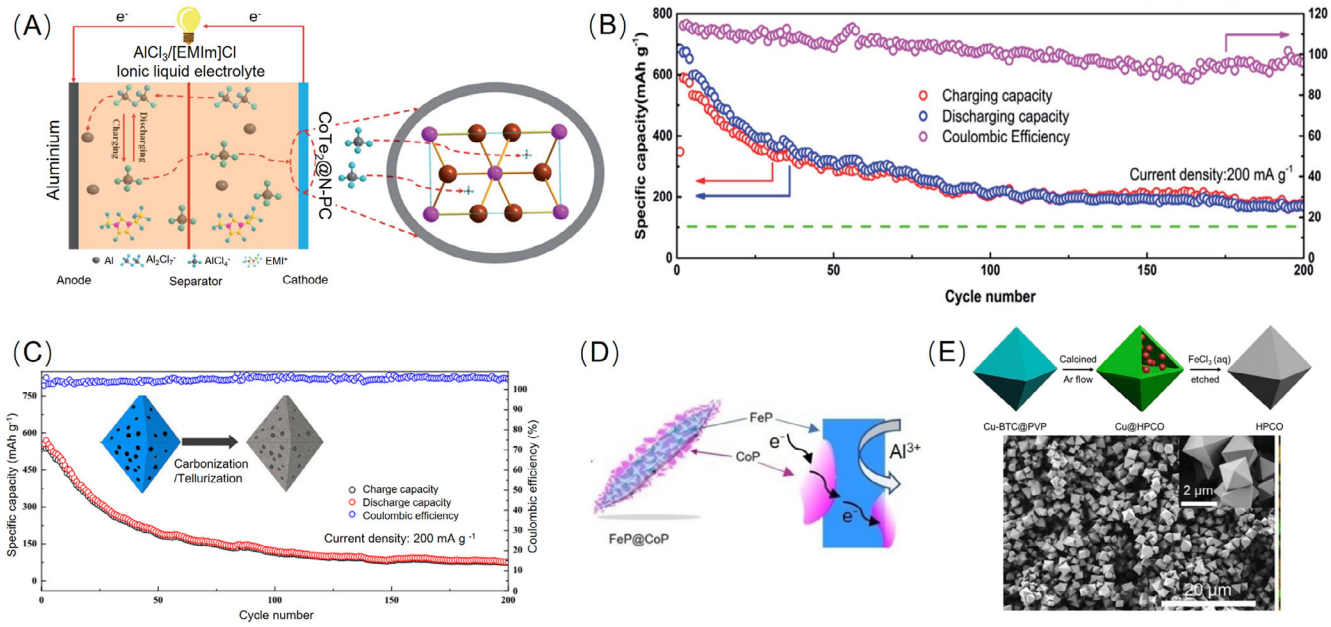

FIGURE 7 | (A) Diagram of the Al/$CoTe_2$@N-PC battery during discharge and charge process. (B) Cycling stability of $CoTe_2$@N-PC at a current density of 200 mA g^{-1}. Reproduced with permission: Copyright 2020, Royal Society of Chemistry [78]. (C) The CuTe@C composite and the battery performance. Reproduced with permission: Copyright 2022, Springer [79]. (D) Pyramidal FeP@CoP and the illustration for electron and ion transportation. Reproduced with permission: Copyright 2023, Wiley-VCH [80]. (E) Cu-BTC@PVP and SEM image. Reproduced with permission: Copyright 2023, Elsevier [81].

paper electrodes. The synthesis involves a two-step process: calcination of the Cu-BTC@PVP precursor followed by etching with $FeCl_3$ solution to remove metallic copper, causing the formation of HPCO. The HPCO structure features a unique hierarchical porous configuration and robust graphitic carbon properties, promoting the insertion and deintercalation of aluminum anions. The battery performance of Al/HPCO is remarkable, maintaining the specific capacity of 60.8 mAh g^{-1} after 200 cycles. Even at a high current density of 1 A g^{-1}, HPCO maintains stable cycling performance over 1000 cycles.

4 | MOFs for Al-S/Se Batteries

Since the exceptional specific capacity of sulfur 1675 mAh g^{-1} and the affordable aluminum, Al-S battery emerges as a highly encouraging energy storage device [82–85]. The charge and discharge range of Al-S batteries is generally between 0.1 and 1.8 V, with a long discharge slope around 0.4 V. In 2015, Cohn et al. first reported on Al-S batteries using non-aqueous electrolytes, demonstrating the high capacity of 1500 mAh g^{-1} [86]. Because of the poor solubility of elemental S, intermediate polysulfides, and final reduction products (Al_2S_3) in IL electrolytes, the electrochemical process between S and Al mainly occurs by a solid state. Consequently, Al-S batteries would present a high overpotential around 1.2 V [87]. Transition metals (e.g., Cu and Co) can profoundly enhance the electrochemical performance of sulfur by providing strong binding to sulfur [30, 88, 89]. MOF or MOF-derived materials offer abundant metal sites to bind sulfur, thereby improving sulfur utilization efficiency.

Guo et al. prepared a cathode material (S@HKUST-1-C) through Cu-stabilized sulfur in microporous carbon (Figure 8A) [90]. The structure contains 10% copper, characterized by a couple of Cu^{2+} ions chelated by four carboxylic acid links. At high temperatures, elemental sulfur permeates into porous HKUST-1-C. The Cu and S can form cluster configurations (Cu_xS) owing to the high activity of Cu nanoparticles at 155°C within S-rich conditions. The robust interaction of Cu and S, combined with the high conductivity of Cu, accelerates the reaction dynamics of S and Al, thus improving the reversibility of S during redox processes. The obvious S_6^{2-} absorption peak was noticed in the discharge state of S@HKUST-1-C, indicating refined sulfur utilization. Therefore, the S@HKUST-1-C as S host shows a high initial discharge capacity of 1200 mAh g^{-1} and provides 460 mAh g^{-1} over 500 cycles (Figure 8B,C). Xiao et al. reported the sulfur host materials using MOF (ZIF-67) for Al batteries [91]. ZIF-67 shows a clear polyhedral shape with a size of approximately 0.8 μm. Co elements are uniformly distributed across the surface of the polyhedron. The S@ZIF-67 composite material can deliver polyhedral morphology similar to ZIF-67 with sharp edges and smooth surfaces. Following high-temperature thermal decomposition, the MOF-derived ZIF-67-700 at 700°C loses its initial crystallinity and is mixed with S to form the S@ZIF-67-700. Notably, S@ZIF-67-700 exhibits a small overpotential of 0.8 V with two flat charge and discharge stages at 1.5 and 0.7 V (Figure 8D), which greatly alleviated the voltage hysteresis behavior. In comparison to the unheated material, S@ZIF-67-700 can display a high first discharge capacity of 693 mAh g^{-1} (Figure 8E). ZIF-67 exhibits strong adsorption to sulfur and intermediate polysulfides (Al_2S_3, Al_2S_6, Al_2S_{12}, and Al_2S_{18}) through electronic interactions, serving as an anchor platform for polysulfides to prevent dissolution and shuttle effects.

In addition, MOFs can be prepared as electrolytes to prevent the dissolution and shuttling of polysulfide in Al-S batteries. Jiao

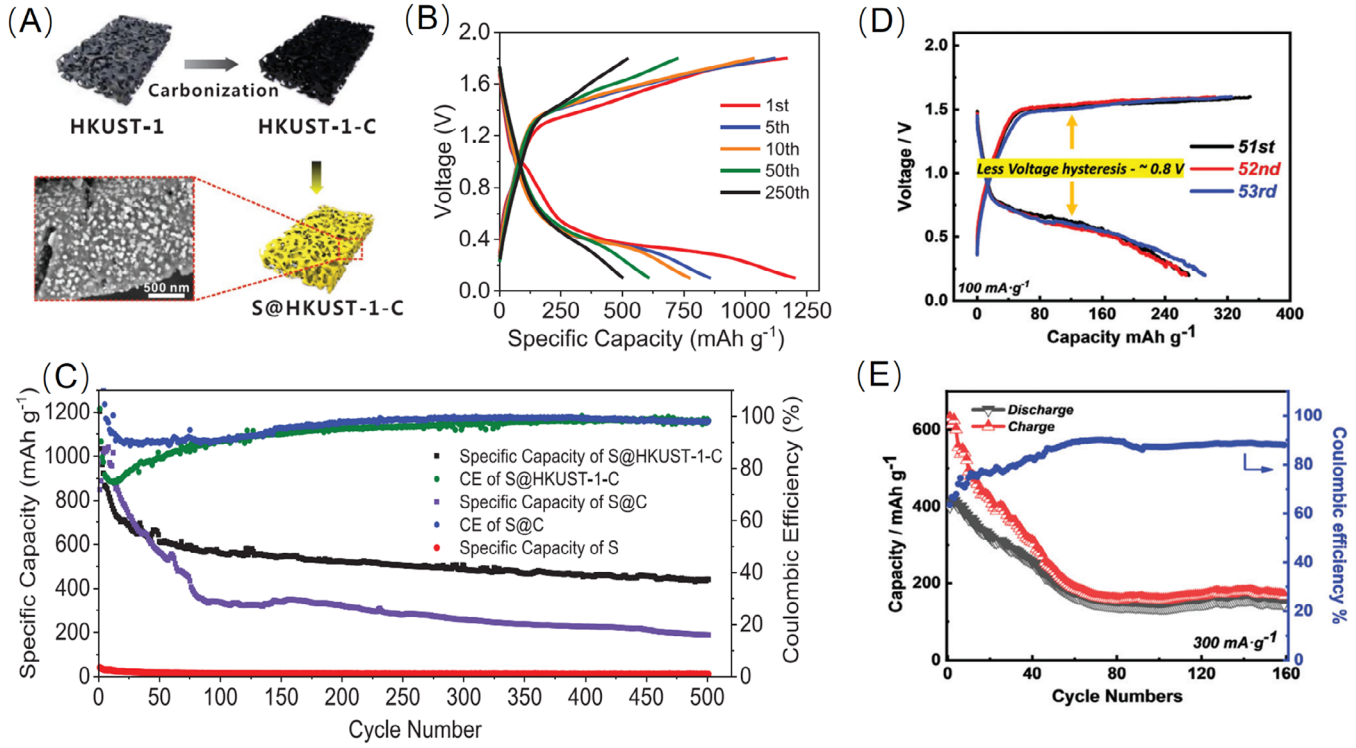

FIGURE 8 | (A) The synthesis procedure for S@HKUST-1-C. (B) The voltage profile of S@HKUST-1-C. (C) Battery performance of S@HKUSTC-1-C, S@C, and S. Reproduced with permission: Copyright 2019, Wiley-VCH [90]. (D) Charge/discharge voltage profiles of S@ZIF-67-700. (E) Cycling performance of S@ZIF-67-700. Reproduced with permission: Copyright 2022, Royal Society of Chemistry [91].

et al. prepared the solid-state electrolyte utilizing the ionic-liquid soaked MOF (IL@MOF) with the gel polyacrylamide electrolyte (MSE@GPE) [92]. Element sulfur was loaded on cobalt nitrogen-doped graphene (S@CoNG). The Co-N_4 structure functions as a versatile catalytic center, continuously facilitating the dissociation of Al^{3+} from Al_xCl_y ions and breaking S-S bonds, significantly enhancing sulfur reaction kinetics (Figure 9A). The charge–discharge profile of the first cycle displayed a discharge voltage plateau at 0.83 V, along with two charge plateaus at 1.42 and 1.55 V. In subsequent cycles, a higher discharge plateau of 0.90 V and a single charge plateau of 1.33 V were observed (Figure 9B). The improved electrolyte penetration into the electrode reduced the overpotential between the charge and discharge processes. Consequently, the electrocatalytically enhanced S@CoNG cathode exhibits a narrow voltage gap of 0.43 V and a high discharge plateau of 0.9 V. The abundant, well-defined MOF channels in IL@MOF, filled with IL, facilitated rapid active ion transport while effectively mitigating the polysulfide shuttling effect, stabilizing the reversible sulfur transformation. The quasi-solid-state Al-S battery, combining the S@CoNG cathode and IL@MOF electrolyte, delivers a high initial specific capacity of 820 mAh g^{-1}, with a capacity retention of 78% after 300 cycles. Subsequently, MSE@GPE was applied in Al-S pouch-cells (Figure 9C) [93]. MSE@GPE solid electrolytes present flexibility and high mechanical strength (Figure 9D). With a mass of 5 mg cm^{-2}, the pouch battery achieves a discharge capacity of 685 mAh g^{-1} and maintains 80% of the capacity over 400 cycles (Figure 9E). The incomplete reaction of the composite S cathode is mainly due to insufficient wettability of the electrolyte. Additionally, the MSE@GPE enhances the current density, resulting in uniform aluminum deposition on metallic surfaces and suppressing the generation of aluminum dendrites and side reactions. 3D depth rendering images show the highlight regions for Al_2S_3 and $AlCl_4$, indicating good adhesion between electrodes and electrolytes (Figure 9F). The stable interface of electrolytes is related to excellent mechanical stability. Meanwhile, Co-NG facilitates the reaction dynamics of sulfur, leading to improved performance of the pouch cell.

Ni and Diao et al. developed Cu-synergistic MoO_2-based nanohybrids as cathodes for RABs by pyrolyzing polyoxomolybdate-based MOFs (POMOFs) [94]. The resulting materials consisted of nanorods encapsulated in porous carbon skeletons, with the nanorods measuring approximately 1 nm in length and 2–3 nm in diameter, while the porous carbon skeletons were around 500 nm. Sulfur was uniformly distributed across the smooth surface (Figure 10A). MoO_2 effectively adsorbed the diffusing polysulfides, while the uniform dispersion of Cu within the carbon matrix created a highly conductive network, enabling rapid charge transfer and facilitating the conversion of polysulfides. During the redox process, aluminum polysulfides oxidize to sulfur at 1.55 V and sulfur reduces to aluminum sulfide at 0.75 V; however, a higher overpotential was still observed (Figure 10B). The synergistic effects of Cu and MoO_2 contributed to an initial battery capacity of 875 mAh g^{-1}, with a capacity retention of 967 mAh g^{-1} at an elevated temperature of 50°C.

Se, a homologous element of sulfur, can deliver a theoretical specific capacity of 679 mAh g^{-1} originating from the conversion mechanism on the generation of $SeCl_4$ during discharge [95, 96]. Se has higher conductivity than sulfur, reaching 1×10^{-3} S m^{-1}. However, aluminum Se (Al-Se) batteries face challenges

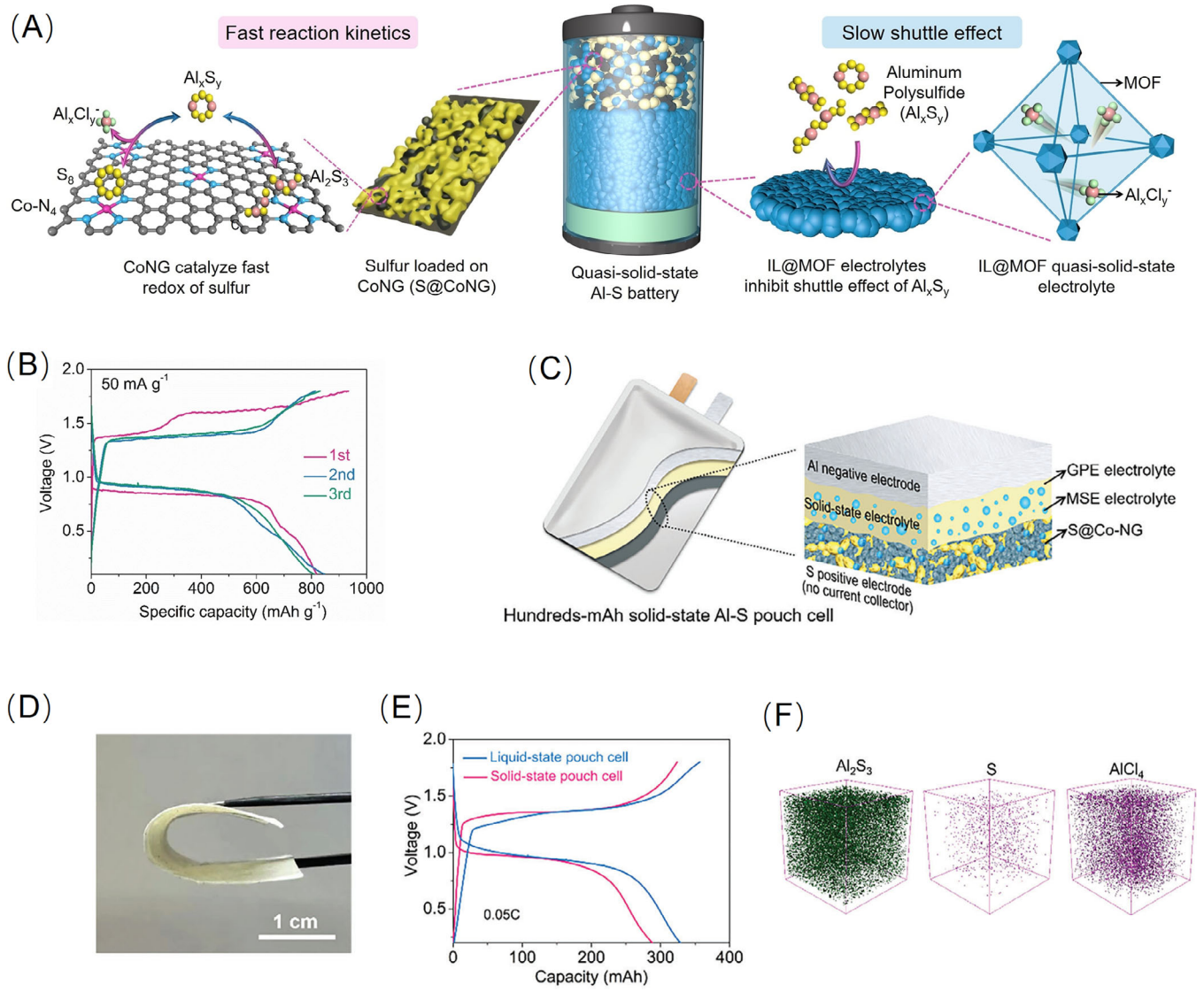

FIGURE 9 | (A) A detailed schematic representation of the quasi-solid-state aluminum sulfur (Al-S) battery, highlighting its operational mechanism. (B) Voltage curves of the first three cycles. Reproduced with permission: Copyright 2022, Wiley-VCH [92]. (C) The structure of Al-S pouch cell with MOF composite solid-state. (D) MSE@GPE solid-state electrolyte sheet. (E) Voltage profiles of liquid and solid-state Al-S pouch cells. (F) The 3D depth images of Al_2S_3, $AlCl_4$, and S ions. Reproduced with permission: Copyright 2023, Wiley-VCH [93].

such as depletion of active materials, degradation of electrode structure, and rapid capacity degradation, which arise from the dissolution of intermediate Se_2Cl_2 in IL-type electrolytes. To solve this issue, significant efforts have been devoted to the research and development of Al-Se batteries [97]. Jiao et al. prepared the quasi-solid-state electrolyte utilizing MOF and gel-polymer electrolyte (MOF@GPE) for Al-Se batteries [98]. Incorporating MOFs into GPEs with robust physical frameworks and ion channels not only suppresses the solubilization of intermediates but also ensures stable ion transport (Figure 10C). The introduced MOFs effectively can trap soluble products, attributed to large surface area and substantial adsorption capacity. The zirconium-based MOF UiO-66, synthesized via the hydrothermal method, was employed as a filler material to fabricate MOF@GPE. SEM analysis revealed that the prepared MOF of octahedral morphology with a uniform particle size of 425 nm. CV testing reveals a reliable electrochemical window of 2.45 V (Figure 10D). Moreover, MOF@GPE exhibits high conductivity of 1.13×10^{-3} S cm^{-1} (Figure 10E). Consequently, Al-Se cell shows an initial specific capacity of 548 mAh g^{-1} and retains 345 mAh g^{-1} over 500 cycles.

5 | Electrolyte

IL electrolytes are exceptionally sensitive to humidity and exhibit poor stability, which can result in gas production, irreversible loss of activity, and unstable electrode interfaces. MOFs can encapsulate a large number of macromolecules and clusters, exerting confinement effects. Encapsulating IL into MOF can protect it from moisture damage. Furthermore, the open uniform channels in MOFs provide ion transport for macromolecules or clusters [99–101]. Jiao et al. reported the semi-solid RAB utilizing IL encapsulated in MOF as an electrolyte [102]. The IL, ([EMIm]Cl): $AlCl_3$ = 1: 1.3, is encapsulated in UiO-67. The size of $AlCl^{4-}$ and $EMIm^+$ ions is 5.3 or 8.5 Å, while the sizes

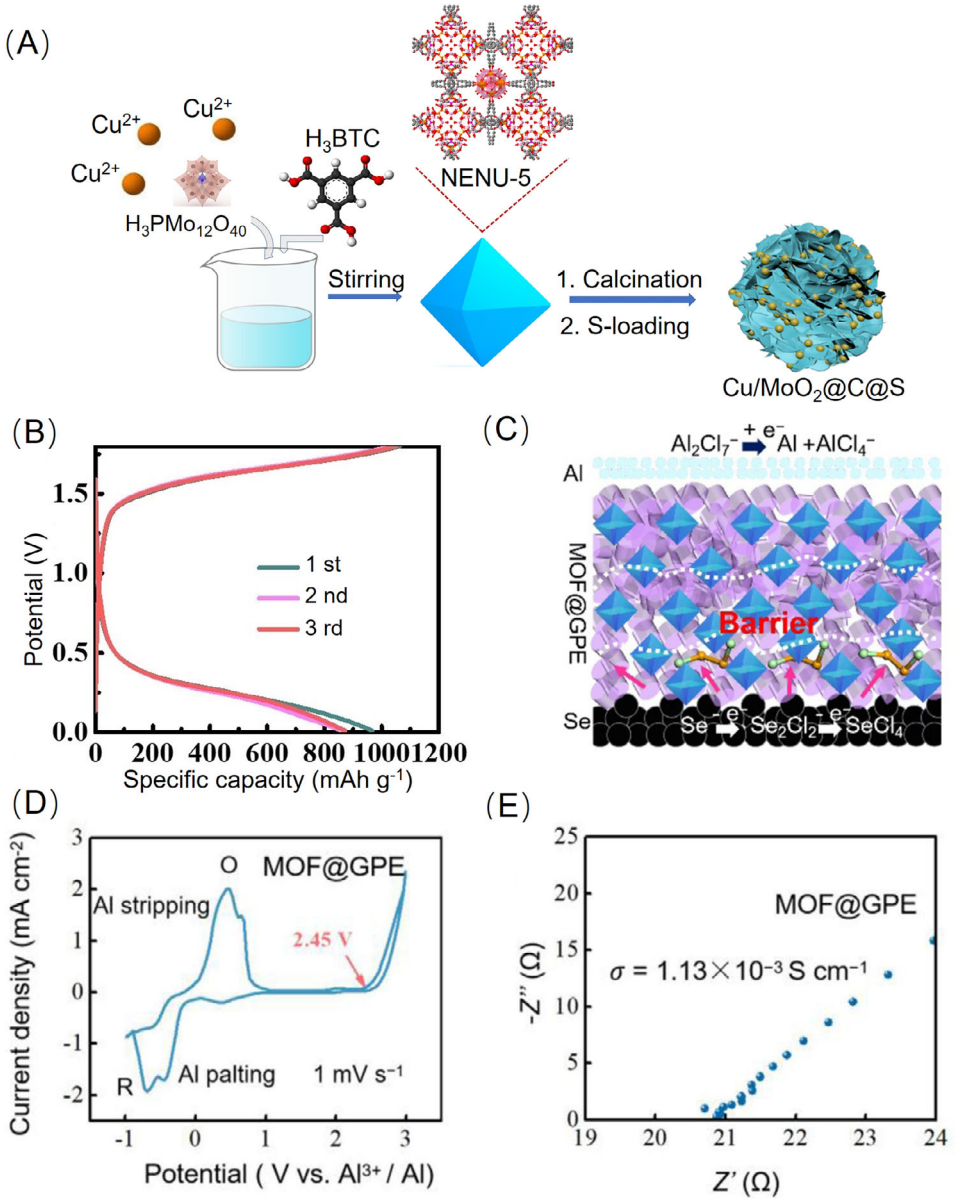

FIGURE 10 | (A) Schematic representation illustrating the synthesis process of the Cu/MoO_2@C@S composite. (B) Voltage profiles with Cu/MoO_2@C@S. Reproduced with permission: Copyright 2024, Wiley-VCH [94]. (C) Al-Se battery with MOF@GPE-1at charge stage. (D) CV profile of the first cycle of Al|MOF@GPE|Mo cell. (E) EIS plot of Mo|MOF@GPE|Mo cell at room temperature. Reproduced with permission: Copyright 2023, Elsevier [98].

of the MOF are approximately 10 and 13 Å, facilitating the infiltration of the IL (Figure 11). The IL@MOF delivers a robust electrochemical window of 0–2.475 V and a high conductivity of 7.5×10^{-4} S cm^{-1}. The battery retains functionality after 2 h of air exposure and successfully passes a fire test. Utilizing IL@MOF as the electrolyte, Al|IL@MOF|Al cell shows two voltage stages at 1.71 and 2.16 V with a polarization voltage of 31 mV and reliable performance beyond 200 h. The Al-graphite cell provides the specific capacity of 75 mA h g^{-1}, exhibiting a prolonged cycle for 2000 cycles.

6 | MOFs for Al-Air Batteries

Al-air batteries provide the advantages of cost-effectiveness, elevated operating voltage (2.7 V), and high theoretical capacity of up to 2.98 Ah g^{-1}, positioning exceptionally promising for practical applications [103–105]. However, designing optimal and long-lasting cathode electrocatalysts for oxygen reduction reactions (ORR) remains challenging such as slow dynamics, poor stability, high cost, and side reactions [106, 107]. Nanomaterials derived from MOFs have emerged as highly promising ORR electrocatalysts and provide the potential to solve these problems because of the large surface area, intrinsic porosity, and rich active sites.

Reported innovations include hybrids of MOFs with carbon materials used as cathodes or catalysts for Al-air batteries. Liu et al. prepared the electrocatalysts ZnO/$ZnCo_2O_4$/C@rGO using ZnO/$ZnCo_2O_4$ loaded onto carbon nanocages and ZIF-67 as a precursor (Figure 12A) [108]. This catalyst exhibits superior electrocatalytic performance, stability, and methanol tolerability in contrast to Pt/C. The elevated surface area of

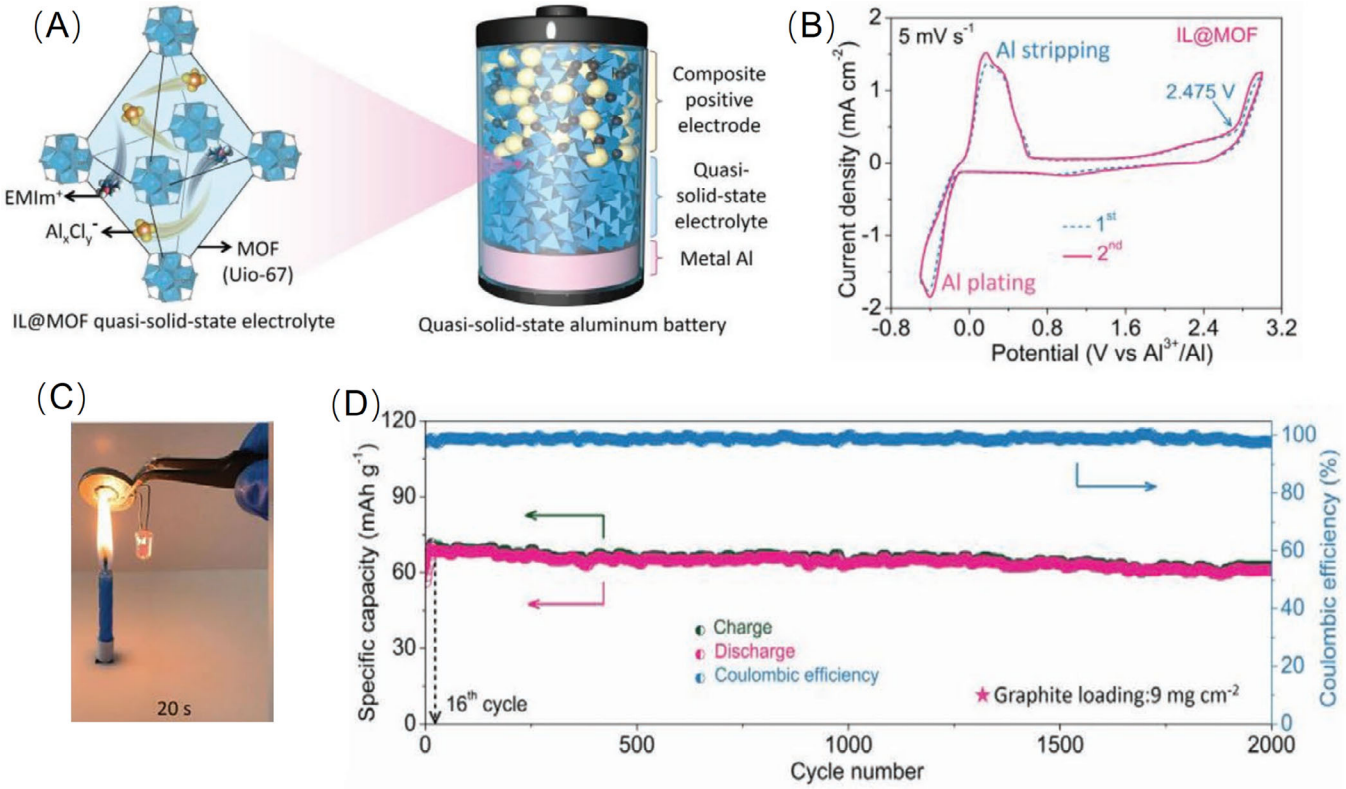

FIGURE 11 | (A) The quasi-solid-state Al battery with IF@MOF electrolyte. (B) CV curve of asymmetric cell Al|IL@MOF|Mo. (C) The burning tests of coin cell while lighting the LED. (D) Cycling performance of the Al|IL@MOF|C battery at 100 mA g^{-1}. Reproduced with permission: Copyright 2022, Wiley-VCH [102].

hollow nanocages offers an increased number of active sites and expanded contact regions. Hollow $ZnO/ZnCo_2O_4/C$, consisting of a multitude of ~5 nm ZnO and $ZnCo_2O_4$ nanoparticles encapsulated within the carbon matrix, enhance oxygen interaction with the exposed nanoparticles, thereby promoting efficient oxygen reduction catalysis. The half-wave potential (E1/2) of $ZnO/ZnCo_2O_4/C$@rGO is −0.15 V, outperforming the Pt/C catalyst (−0.18 V), signaling rapid ORR kinetics (Figure 12B). The composite as cathodic catalyst of Al-air cell shows the specific capacity of 42.6 mAh g^{-1} corresponding to the power density of 1.41 mW cm^{-2}. Furthermore, metal-coordinated N-doped carbon frameworks are utilized as ORR activators owing to their exceptional activity and durability. Copper-centered MOF (Cu-MOFs) can act as a self-sacrificial agent for modifying Ketjen black (KB) carbon (Figure 12C) [109]. The Cu-MOF/KB derivative, CuNC/KB-400, comprises Cu_2O, metallic Cu nanoparticles, and amorphous CuN_xC_y fragments. This complex catalyst demonstrates enhanced ORR catalytic performance relative to reversible hydrogen electrodes (RHE), with an E1/2 of 0.82 V. By employing it as the cathode catalyst, the cell provides a higher and more stable voltage of 1.53 V, in contrast to the 1.45 V observed with the commercial Pt/C catalyst (Figure 12D).

Further advances involve combining MOFs with transition bimetallic to prepare composite materials that improve catalytic performance. Wang et al. prepared N, S co-doped porous carbon and definitely nickel-cobalt sulfide (Ni-Co-S@G/NSC) utilizing 3D MOF precursor (Figure 12E) [110]. The MOF, NH_2-MIL-101 with a spacious pore system provides high chemical stability, making it suitable as a host precursor. The robust interaction of Ni-Co-S enhances electron transfer and catalytic performance. The Ni-Co-S@G/NSC900 demonstrates a notable cathodic peak at 0.822 V versus RHE, outperforming the Pt/C of 0.728 V. Utilizing Ni-Co-S@G/NSC900 as catalyst, the Al-air cell achieves an impressive capacity of 2947 mAh g^{-1} and high discharge voltage at 1.23 V (Figure 12F). Pomegranate peel extract (PPE) can be incorporated into aluminum-based MOFs (Al-MOFs) to create the sensor Al-MOF-PPE, capable of detecting carcinogenic Cr(VI) and converting it into the less harmful Cr(III) [111]. The resulting Al-MOF-PPE-Cr(III) complex functions as a corrosion inhibitor for metal surfaces, exhibiting both cathodic and anodic inhibition properties. This dual-inhibition mechanism ensures the protection of aluminum electrodes in Al-air batteries for up to 220 min. However, further research is required to enhance its overall performance in Al-air battery applications.

Iron single-atom modified nitrogen carbon sheets were prepared on carbon cloth (Fe-SA-NC@CC) using ferrocene and Zn-based MOF as self-supporting electrodes (Figure 13A) [112]. Zn MOF presents a uniform triangular sheet-like pattern that covers carbon cloth. At elevated temperatures, ferrocene framework forms Fe-N bonds and the nitrogen of MOF. This material provides fast ion/electron transfer, enabling high ORR activity. In hydrogel-based flexible Al-air batteries, this arrangement achieves a high power density of 3.94 mW cm^{-2} (Figure 13B). Additionally, the cell exhibits an open circuit voltage of 2.1 V and a discharge voltage of around 1.5 V over 8 h.

Carbon matrices-based organic also serve as excellent hosts for oxygen catalysts. Cui et al. reported the dicyandiamide

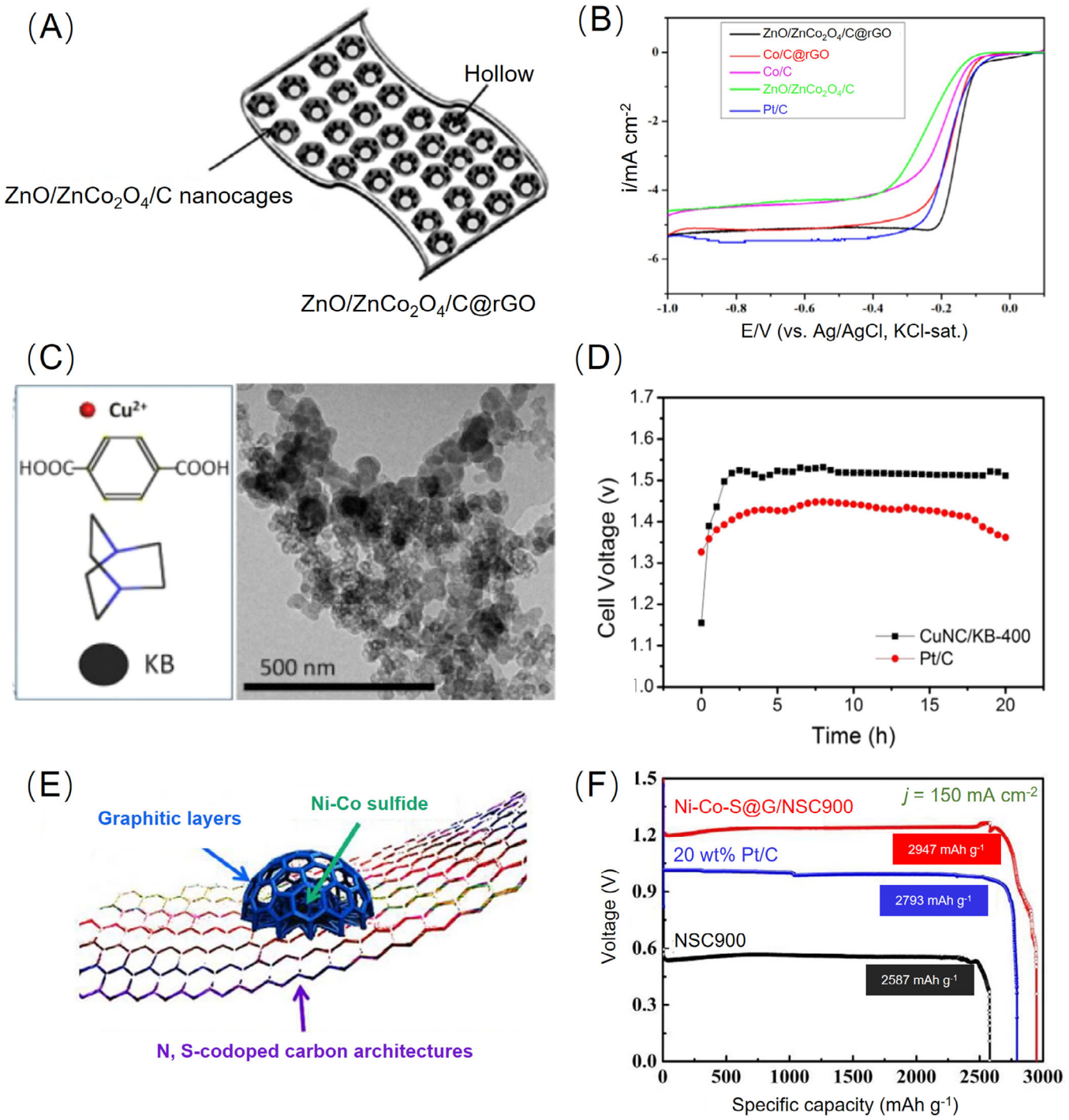

FIGURE 12 | (A) The structure of $ZnO/ZnCo_2O_4/C@rGO$ hybrids. (B) LSV profile of different catalysts. Reproduced with permission: Copyright 2017, American Chemical Society [108]. (C) The Cu-MOF/Ketjen black (KB)-derived catalyst. (D) The constant current discharge profile for Al-air batteries employing Pt/C and CuNC/KB catalysts. Reproduced with permission: Copyright 2017, American Chemical Society [109]. (E) The configuration of mesoporous Ni-Co-S@G/NSC. (F) Polarization curves and corresponding specific capacity of Al-air batteries with different catalysts. Reproduced with permission: Copyright 2017, Elsevier [110].

(DCDA) as the C and N source to regular configuration of MOF-based porous carbon (Figure 13C) [113]. An N-doped graphite carbon framework coating FeCo nanoparticles (PD-800) was prepared by combining DCDA and $Fe_3[Co(CN)_6]_2$. This combination of FeCo and N-doped graphite yields excellent ORR activity and durability. Meanwhile, PD-800 consists of FeCo alloy incorporated into nitrogen-doped graphite carbon shells. With the surface area of 203.41 $m^2\ g^{-1}$, PD-800 exposes a substantial number of active sites, thereby enhancing its electrocatalytic ability. The pyridinic N, metal (Fe/Co)-N_x, and pyrrolic-N contribute to an improved starting voltage. The cell with PD-800 catalyst produces an open circuit voltage of 1.68 V, exceeding 1.65 V of Pt/C. Based on the transfer of four electrons, the PD-800 battery showcases a specific capacity

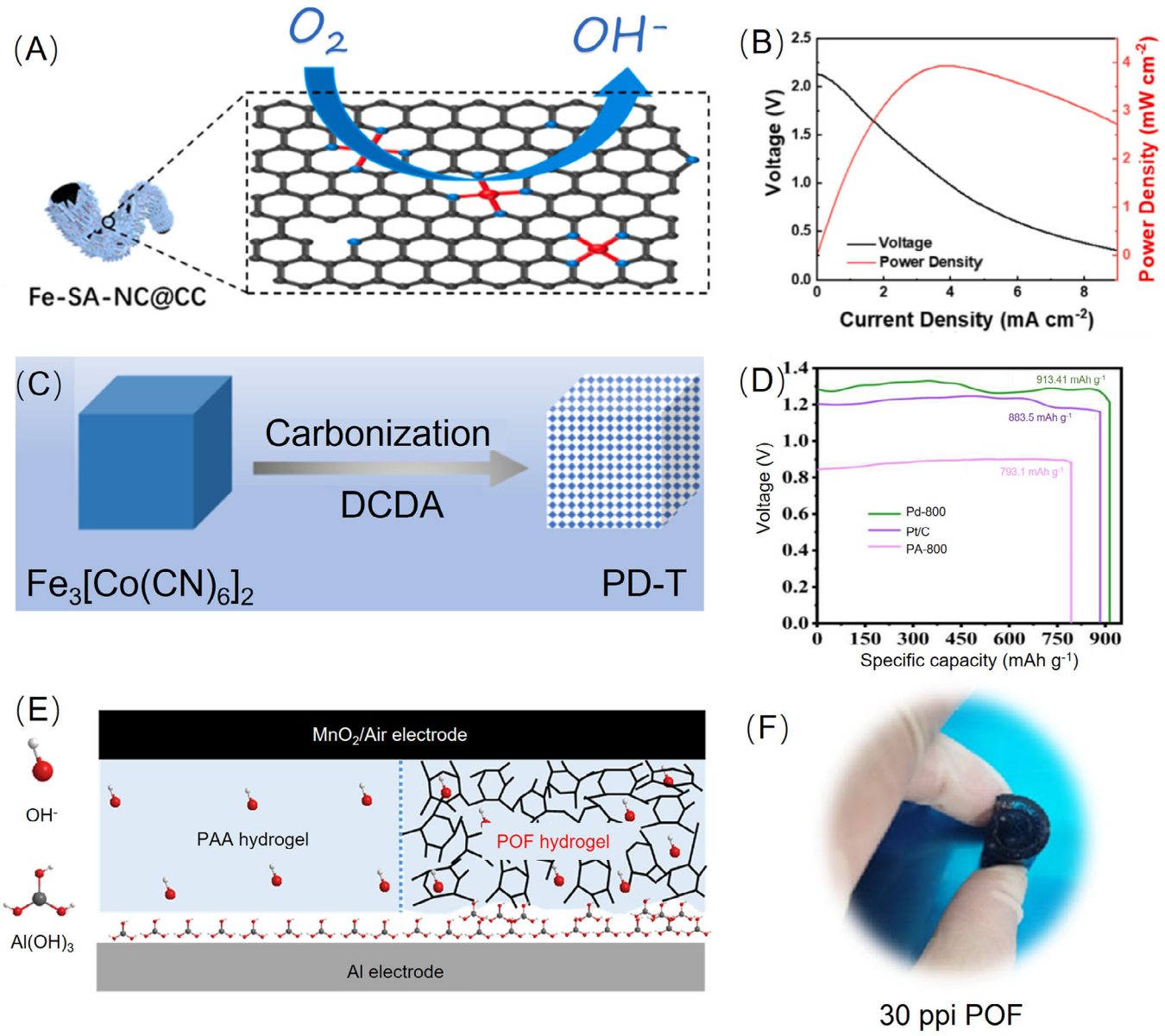

FIGURE 13 | (A) The configuration of Fe-SA-NC@CC, (B) Work voltage and power density of Fe-SA-NC@CC-based cell. Reproduced with permission: Copyright 2021, Elsevier [112]. (C) The fabrication procedure of PD-T catalyst. (D) Specific capacities of employing three cathodes. Reproduced with permission: Copyright 2020, Elsevier [113]. (E) The enhanced mechanism diagram of the working time, (F) Flexibility tests of POF. Reproduced with permission: Copyright 2017, Royal Society of Chemistry [114].

of 913.41 mAh g^{-1} with a power density of 98.62 mW cm^{-2} (Figure 13D).

Pristine MOF aluminum terephthalate (AT) is another viable option as the cathode material [114]. Utilizing the composite of AT and conductive carbon, the Al-air battery delivers specific capacities of 87, 77, and 57 mAh g^{-1} in the 1st, 5th, and 25th cycles, respectively. The MOFs provide a path for the transmission of aluminum ions and oxygen. However, Al_2O_3 and $Al(OH)_3$ detected as byproducts during electrochemical redox processes would deteriorate the MOF surface. To address the issues of self-corrosion, electrical leakage, and massive accumulation typical in Al-air batteries, a hydrogel electrolyte has been developed (Figure 13E). The conductivity of the hydrogel closely approximates that of liquid electrolytes. For example, a polyurethane organic framework (POF) was reported as the internal hold structure for polyacrylic acid (PAA) hydrogel [115]. The participation of POF can provide PAA hydrogel with high mechanical strength and toughness. Even under extrusion, the POF hydrogel maintains structural integrity, providing a tensile stress of 49.5 kPa at 30 ppi (Figure 13F). With the 20 ppi POF, the discharge capacity of the cell increases by 79 mAh cm^{-2}.

7 | Conclusions and Prospects

In summary, MOFs, with their distinctive physical and chemical properties, present a substantial impact on RAB development

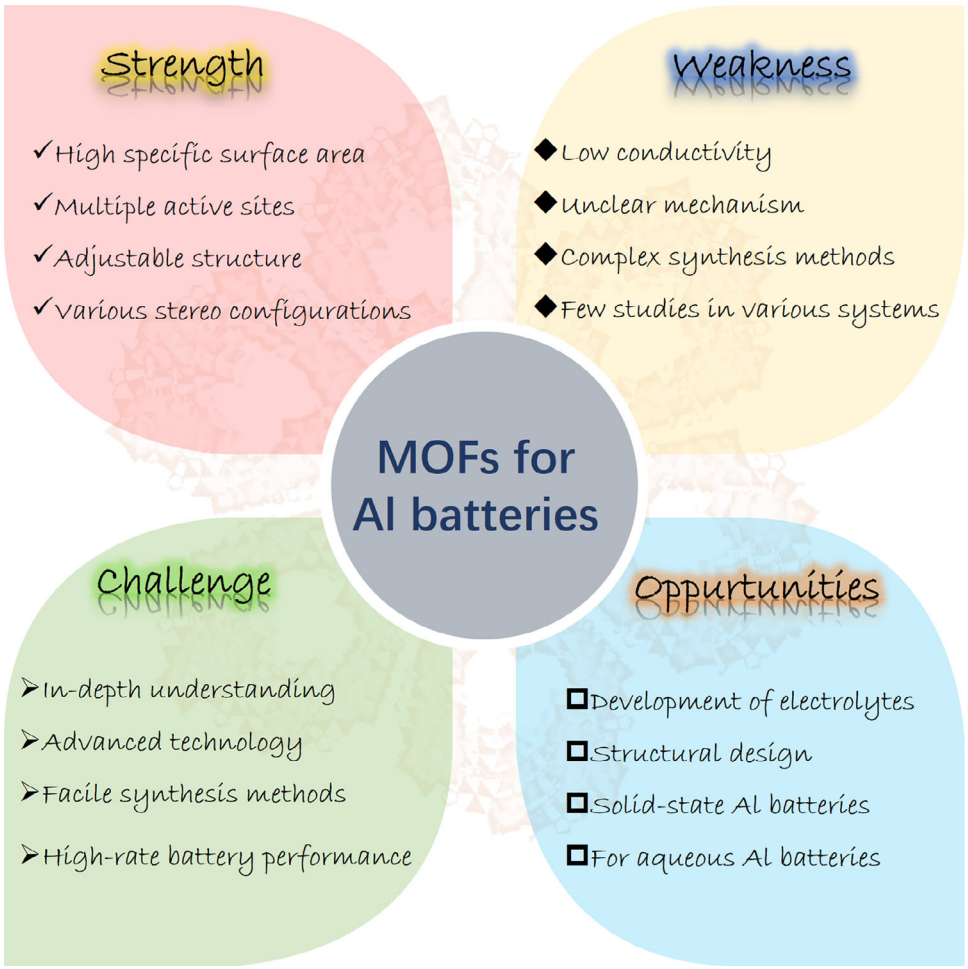

FIGURE 14 | Opportunities and challenges of MOFs in aluminum batteries for the future.

and have garnered considerable attention. This review has highlighted the diverse roles that MOFs play within the realm of aluminum batteries. Pristine MOFs, with multiple pores and channels, facilitate efficient ion insertion and extraction. The abundant active sites provided by organic ligands and metal ions in MOFs ensure high capacity and enable dynamic valence changes during electrochemical reactions, essential for maintaining robust battery performance. MOF-derived materials with diverse metal and active components deliver high specific capacity and reliability. For Al-S/Se cells, S and Se as cathode can exhibit the high theoretical specific capacity of 1675 and 679 mAh g^{-1}. The MOFs act as host substrates, absorbing sulfides and selenides to improve battery performance. Furthermore, MOFs function as excellent catalysts in Al-air batteries, improving the dynamics of oxygen reduction via accelerated redox reactions. Therefore, MOFs contribute significantly to the advancement of RABs with huge potential for application in next-generation energy systems.

Despite these advances, some obstacles remain that may impede the optimal performance of MOFs in RABs. For example, the intrinsic low conductivities of MOFs limit reaction dynamics and rate performance, necessitating the inclusion of conductive additives like carbon-based materials or conductive polymers. Additionally, the structural robustness of MOFs during redox remains a critical concern, as the MOF framework is prone to collapse in redox reactions. Therefore, to further the development of MOFs in RABs, we propose several future directions (Figure 14):

1. Mechanistic understanding of the electrochemical processes of MOFs in RABs: Unlike lithium and sodium ion batteries, RABs, which are multivalent metal ion batteries, go through complex redox transformations involving multiple electron exchanges and valence states. The intake and release of Al ions and Al anion groups during redox process, along with the changing valence of metal ions in MOFs, are crucial but poorly understood characteristics. A detailed understanding of these processes is crucial, especially because the behavior of MOFs various organic ligands and metal ions remains to be fully characterized in RABs.
2. Develop advanced characterization methods: To achieve a more comprehensive understanding of the structural and chemical behavior of MOFs during battery operation, the application of advanced characterization techniques is essential. In situ characterization approaches are especially useful since they enable real-time observation of dynamic changes in MOFs under operational conditions. Furthermore, modern techniques such as time-of-flight secondary ion mass spectrometry (TOF-SIMS) and atom probe tomography (APT) allow for thorough investigations of material composition and 3D atomic organization. Employing these

sophisticated methodologies will enhance our understanding of the structural evolution of MOFs, ensuring a more accurate prediction of their performance in RABs.

3. Facile preparation of novel and stable MOFs: The synthesis of some MOFs requires expensive raw materials, complex ligand synthesis processes, and high-temperature conditions. It is critical to develop methods for creating MOFs that are not only cost-effective but also environmentally benign and straightforward. Certain MOFs undergo structural degradation during electrochemical redox processes, particularly in acidic aluminum electrolytes, resulting in accelerated capacity loss and reduced cycle life. Establishing synthesis protocols that enhance the structural robustness of MOFs is essential for advancing their application in RABs, thereby ensuring improved battery performance. MOF structure incorporates ligands with conjugated π electron systems, highly conductive metals such as Cu and Ni, and appropriately sized pores, all of which facilitate electrolyte ion transport, leading to enhanced conductivity.
4. Develop MOFs for aqueous RABs: The current report on MOFs used for aqueous RABs is scarce. Aqueous batteries provide notable benefits, including low cost, environmental friendliness, and elevated safety. Nevertheless, their practical implementation is restricted due to a narrow voltage window and slow electrochemical kinetics. MOFs, with their diverse ligands and metal ion centers, have the potential to overcome these constraints.
5. MOFs as solid electrolytes or anode protective layers: Although the formation of aluminum dendrites is not commonly reported, aluminum electrodes are susceptible to corrosion during electrochemical redox reactions, which can significantly degrade cycle performance. By applying MOFs as protective coatings on the aluminum anode, their frame configuration can regulate the uniform deposition of aluminum ions, promoting a more stable and homogeneous aluminum surface. This approach not only prevents electrode deterioration but also enhances the overall battery performance and longevity.

MOF materials, characterized by their high specific surface area, tunable pore structure, multifunctionality, excellent chemical stability, and metal-organic synergy, hold significant promise for aluminum batteries. However, considerable challenges remain before their practical application can be fully realized. As previously mentioned, MOFs exhibit great potential in this field. Future research should prioritize the optimization of MOF structures and functionalities to enhance specific capacity and overall battery performance. Additionally, improving the intrinsic conductivity of MOFs for potential use as electrolytes, and exploring their applications in aqueous aluminum batteries and solid-state aluminum batteries, will be essential directions for further development.

Compared to lithium, sodium, and zinc batteries, there is a selection of electrode materials suitable for RABs. Despite this, with their diverse functions and ability to augment electrochemical performance, MOFs as battery materials hold the potential to revolutionize RAB systems. Continued research and development inspired by this review could lead to breakthroughs and advanced RABs in the future.

Acknowledgments

The authors acknowledge the funding support from the ASTAR MTC programmatic project under Grant No. M23L9b0052, Indonesia-NTU Singapore Institute of Research for Sustainability and Innovation (INSPIRASI) under contract no. 6635/E3/KL.02.02/2023, and Singapore NRF Singapore-China flagship program under grant no. 023740-00001.

Conflicts of Interest

The authors declare no conflict of interest.

References

1. M. Armand and J. M. Tarascon, "Building Better Batteries," *Nature* 451, no. 7179 (2008): 652–657.
2. Y. K. Sun, S. T. Myung, B. C. Park, et al., "High-Energy Cathode Material for Long-life and Safe Lithium Batteries," *Nature Materials* 8, no. 4 (2009): 320–324.
3. B. Scrosati, J. Hassoun, and Y.-K. Sun, "Lithium-Ion Batteries. A Look Into the Future," *Energy & Environmental Science* 4, no. 9 (2011): 3287–3295.
4. A. Manthiram, "Materials Challenges and Opportunities of Lithium Ion Batteries," *Journal of Physical Chemistry Letters* 2, no. 3 (2011): 176–184.
5. J. B. Goodenough and Y. Kim, "Challenges for Rechargeable Li Batteries," *Chemistry of Materials* 22, no. 3 (2009): 587–603.
6. B. L. Ellis, K. T. Lee, and L. F. Nazar, "Positive Electrode Materials for Li-ion and Li-batteries," *Chemistry of Materials* 22, no. 3 (2010): 691–714.
7. J. W. Fergus, "Recent Developments in Cathode Materials for Lithium Ion Batteries," *Journal of Power Sources* 195, no. 4 (2010): 939–954.
8. M. S. Whittingham, "Lithium Batteries and Cathode Materials," *Chemistry of Materials* 104, no. 10 (2004): 4271–4301.
9. D. Bruce, K. Haresh, and J. M. Tarascon, "Electrical Energy Storage for the Grid: A Battery of Choices," *Science* 334 (2011): 928–935.
10. Z. Yang, J. Zhang, M. C. Kintner-Meyer, et al., "Electrochemical Energy Storage for Green Grid," *Chemical Reviews* 111, no. 5 (2011): 3577–3613.
11. G. A. Elia, K. Marquardt, K. Hoeppner, et al., "An Overview and Future Perspectives of Aluminum Batteries," *Advanced Materials* 28, no. 35 (2016): 7564–7579.
12. H. Yang, H. Li, J. Li, et al., "The Rechargeable Aluminum Battery: Opportunities and Challenges," *Angewandte Chemie International Edition* 58, no. 35 (2019): 11978–11996.
13. X. Zhang, Y. Tang, F. Zhang, and C. S. Lee, "A Novel Aluminum-graphite Dual-ion Battery," *Advanced Energy Materials* 6, no. 11 (2016): 1502588.
14. M. C. Lin, M. Gong, B. Lu, et al., "An Ultrafast Rechargeable Aluminium-ion Battery," *Nature* 520, no. 7547 (2015): 325–328.
15. A. Vahid Mohammadi, A. Hadjikhani, S. Shahbazmohamadi, and M. Beidaghi, "Two-Dimensional Vanadium Carbide (MXene) as a High-Capacity Cathode Material for Rechargeable Aluminum Batteries," *ACS Nano* 11, no. 11 (2017): 11135–11144.
16. C. Li, C. C. Hou, L. Chen, S. Kaskel, and Q. Xu, "Rechargeable Al-ion Batteries," *EnergyChem* 3, no. 2 (2021): 100049.
17. V. Shrivastav, S. Sundriyal, P. Goel, et al., "Metal-Organic Frameworks (MOFs) and Their Composites as Electrodes for Lithium Battery Applications: Novel Means for Alternative Energy Storage," *Coordination Chemistry Reviews* 393 (2019): 48–78.

18. M. Angell, C. J. Pan, Y. Rong, et al., "High Coulombic Efficiency Aluminum-Ion Battery Using an $AlCl_3$-urea Ionic Liquid Analog Electrolyte," *Proceedings National Academy of Science USA* 114, no. 5 (2017): 834–839.

19. J. V. Rani, V. Kanakaiah, T. Dadmal, M. S. Rao, and S. Bhavanarushi, "Fluorinated Natural Graphite Cathode for Rechargeable Ionic Liquid Based Aluminum-ion Battery," *Journal of the Electrochemical Society* 160, no. 10 (2013): A1781–A1784.

20. M. Jiang, C. Fu, P. Meng, et al., "Challenges and Strategies of Low-cost Aluminum Anodes for High-Performance Al-based Batteries," *Advanced Materials* 34, no. 2 (2022): e2102026.

21. Y. Zhang, S. Liu, Y. Ji, J. Ma, and H. Yu, "Emerging Nonaqueous Aluminum-ion Batteries: Challenges, Status, and Perspectives," *Advanced Materials* 30, no. 38 (2018): e1706310.

22. H. Chen, F. Guo, Y. Liu, et al., "A Defect-free Principle for Advanced Graphene Cathode of Aluminum-Ion Battery," *Advanced Materials* 29, no. 12 (2017): 1605958.

23. F. Wu, H. Yang, Y. Bai, and C. Wu, "Paving the Path Toward Reliable Cathode Materials for Aluminum-ion Batteries," *Advanced Materials* 31, no. 16 (2019): e1806510.

24. S. Gu, H. Wang, C. Wu, et al., "Confirming Reversible Al^{3+} Storage Mechanism Through Intercalation of Al^{3+} Into V_2O_5 Nanowires in a Rechargeable Aluminum Battery," *Energy Storage Materials* 6 (2017): 9–17.

25. L. Zhang, L. Chen, H. Luo, X. Zhou, and Z. Liu, "Large-Sized Few-Layer Graphene Enables an Ultrafast and Long-life Aluminum-Ion Battery," *Advanced Energy Materials* 7, no. 15 (2017): 1700034.

26. G. A. Elia, K. V. Kravchyk, M. V. Kovalenko, et al., "An Overview and Prospective on Al and Al-Ion Battery Technologies," *Journal of Power Sources* 481 (2021): 228870.

27. W. Xia, A. Mahmood, R. Zou, and Q. Xu, "Metal-Organic Frameworks and Their Derived Nanostructures for Electrochemical Energy Storage and Conversion," *Energy & Environmental Science* 8, no. 7 (2015): 1837–1866.

28. L. Wang, Y. Han, X. Feng, et al., "Metal-Organic Frameworks for Energy Storage: Batteries and Supercapacitors," *Coordination Chemistry Reviews* 307 (2016): 361–381.

29. Y. Zhao, Z. Song, X. Li, et al., "Metal Organic Frameworks for Energy Storage and Conversion," *Energy Storage Materials* 2 (2016): 35–62.

30. S. Bai, X. Liu, K. Zhu, S. Wu, and H. Zhou, "Metal-Organic Framework-based Separator for Lithium-sulfur Batteries," *Nature Energy* 1, no. 7 (2016): 16094.

31. Z. Wang, J. Huang, Z. Guo, et al., "A Metal-Organic Framework Host for Highly Reversible Dendrite-free Zinc Metal Anodes," *Joule* 3, no. 5 (2019): 1289–1300.

32. W. Li, S. Hu, X. Luo, et al., "Confined Amorphous Red Phosphorus in MOF-derived N-Doped Microporous Carbon as a Superior Anode for Sodium-Ion Battery," *Advanced Materials* 29, no. 16 (2017): 1605820.

33. D. Wu, Z. Guo, X. Yin, et al., "Metal-Organic Frameworks as Cathode Materials for Li-O_2 Batteries," *Advanced Materials* 26, no. 20 (2014): 3258–3262.

34. S. Sanati, R. Abazari, J. Albero, et al., "Metal-Organic Framework Derived Bimetallic Materials for Electrochemical Energy Storage," *Angewandte Chemie International Edition* 60, no. 20 (2021): 11048–11067.

35. Y. S. Wei, M. Zhang, R. Zou, and Q. Xu, "Metal-Organic Framework-Based Catalysts With Single Metal Sites," *Chemical Reviews* 120, no. 21 (2020): 12089–12174.

36. D. J. Kim, D. J. Yoo, M. T. Otley, et al., "Rechargeable Aluminium Organic Batteries," *Nature Energy* 4, no. 1 (2018): 51–59.

37. D. Y. Wang, R. Liu, W. Guo, G. Li, and Y. Fu, "Recent Advances of Organometallic Complexes for Rechargeable Batteries," *Coordination Chemistry Reviews* 429 (2021): 213650.

38. G. Xu, P. Nie, H. Dou, et al., "Exploring Metal Organic Frameworks for Energy Storage in Batteries and Supercapacitors," *Materials Today* 20, no. 4 (2017): 191–209.

39. Q. Zhang, S. Jiang, T. Lv, Y. Peng, and H. Pang, "Application of Conductive MOF in Zinc-based Batteries," *Advanced Materials* 35, no. 48 (2023): e2305532.

40. T. Zhao, H. Wu, X. Wen, et al., "Recent Advances in MOFs/MOF Derived Nanomaterials Toward High-Efficiency Aqueous Zinc Ion Batteries," *Coordination Chemistry Reviews* 468 (2022): 214642.

41. Z. Xie, W. Xu, X. Cui, and Y. Wang, "Recent Progress in Metal-Organic Frameworks and Their Derived Nanostructures for Energy and Environmental Applications," *Chemsuschem* 10, no. 8 (2017): 1645–1663.

42. R. Zhao, Y. Wu, Z. Liang, et al., "Metal-Organic Frameworks for Solid-State Electrolytes," *Energy & Environmental Science* 13, no. 8 (2020): 2386–2403.

43. A. Morozan and F. Jaouen, "Metal Organic Frameworks for Electrochemical Applications," *Energy & Environmental Science* 5, no. 11 (2012): 9269–9290.

44. Z. Liang, C. Qu, W. Guo, R. Zou, and Q. Xu, "Pristine Metal-Organic Frameworks and Their Composites for Energy Storage and Conversion," *Advanced Materials* 30, no. 37 (2018): e1702891.

45. A. E. Baumann, D. A. Burns, B. Liu, and V. S. Thoi, "Metal-Organic Framework Functionalization and Design Strategies for Advanced Electrochemical Energy Storage Devices," *Communications Chemistry* 2, no. 1 (2019): 86.

46. C. Wang, Y. V. Kaneti, Y. Bando, et al., "Metal-Organic Framework-Derived One-dimensional Porous or Hollow Carbon-Based Nanofibers for Energy Storage and Conversion," *Materials Horizons* 5, no. 3 (2018): 394–407.

47. M. Shen and H. Ma, "Metal-Organic Frameworks (MOFs) and Their Derivative as Electrode Materials for Lithium-ion Batteries," *Coordination Chemistry Reviews* 470 (2022): 214715.

48. D.-S. Bin, Z.-L. Zheng, A.-M. Cao, and L.-J. Wan, "Template-Free Synthesis of Hollow Carbon-based Nanostructures From MOFs for Rechargeable Battery Applications," *Science China Chemistry* 66, no. 1 (2022): 65–77.

49. R. Razaq, M. M. U. Din, D. R. Småbråten, et al., "Synergistic Effect of Bimetallic MOF Modified Separator for Long Cycle Life Lithium-Sulfur Batteries," *Advanced Energy Materials* 14, no. 3 (2023): 2302897.

50. J. Zhang, Y. Wang, Q. Xia, et al., "Confining Polymer Electrolyte in MOF for Safe and High-performance All-Solid-State Sodium Metal Batteries," *Angewandte Chemie International Edition* 63, no. 16 (2024): e202318822.

51. J. Zhou, X. Yu, J. Zhou, and B. Lu, "Polyimide/Metal-Organic Framework Hybrid for High Performance Al-Organic Battery," *Energy Storage Materials* 31 (2020): 58–63.

52. T. Xiong, B. He, and T. Zhou, "Stretchable Fiber-Shaped Aqueous Aluminum Ion Batteries," *EcoMat* 4, no. 5 (2022): e12218.

53. X. Han, S. Li, W. L. Song, et al., "Stable High-Capacity Organic Aluminum-porphyrin Batteries," *Advanced Energy Materials* 11, no. 32 (2021): 2101446.

54. Y. Guo, W. Wang, H. Lei, M. Wang, and S. Jiao, "Alternate Storage of Opposite Charges in Multisites for High-Energy-Density Al-MOF Batteries," *Advanced Materials* 34, no. 13 (2022): e2110109.

55. D. Pakulski, V. Montes-García, A. Gorczyński, et al., "Two-Dimensional Metal-organic Polymers as Cathode Hybrid Materials for High-Performance Al-Batteries," *Journal of Materials Chemistry A* 12, no. 1 (2024): 440–450.

56. S. Yang, C. Li, H. Lv, et al., "High-Rate Aqueous Aluminum-Ion Batteries Enabled by Confined Iodine Conversion Chemistry," *Small Methods* 5, no. 10 (2021): e2100611.

57. X. Cao, C. Tan, M. Sindoro, and H. Zhang, "Hybrid Micro-/Nano-Structures Derived From Metal-Organic Frameworks: Preparation and Applications in Energy Storage and Conversion," *Chemical Society Reviews* 46, no. 10 (2017): 2660–2677.

58. L. Yang, X. Zeng, W. Wang, and D. Cao, "Recent Progress in MOF-derived, Heteroatom-doped Porous Carbons as Highly Efficient Electrocatalysts for Oxygen Reduction Reaction in Fuel Cells," *Advanced Functional Materials* 28, no. 7 (2017): 1704537.

59. F. Zou, X. Hu, Z. Li, et al., "MOF-derived Porous ZnO/$ZnFe_2O_4$/C Octahedra With Hollow Interiors for High-Rate Lithium-Ion Batteries," *Advanced Materials* 26, no. 38 (2014): 6622–6628.

60. Y. Fu, Q. Wei, G. Zhang, et al., "High-Performance Reversible Aqueous Zn-ion Battery Based on Porous MnO_x Nanorods Coated by MOF-derived N-Doped Carbon," *Advanced Energy Materials* 8, no. 26 (2018): 1801445.

61. M. Zhang, Q. Dai, H. Zheng, M. Chen, and L. Dai, "Novel MOF-Derived Co@N-C Bifunctional Catalysts for Highly Efficient Zn-Air Batteries and Water Splitting," *Advanced Materials* 30, no. 10 (2018): 1705431.

62. X. Xiao, M. Wang, J. Tu, Y. Luo, and S. Jiao, "Metal-Organic Framework-Derived Co_3O_4@MWCNTs Polyhedron as Cathode Material for a High-Performance Aluminum-Ion Battery," *ACS Sustainable Chemistry & Engineering* 7, no. 19 (2019): 16200–16208.

63. K. Zhang, T. H. Lee, J. H. Cha, et al., "Metal-Organic Framework-Derived Metal Oxide Nanoparticles@Reduced Graphene Oxide Composites as Cathode Materials for Rechargeable Aluminium-Ion Batteries," *Scientific Reports* 9, no. 1 (2019): 13739.

64. C. Li, S. Dong, R. Tang, et al., "Heteroatomic Interface Engineering in MOF-derived Carbon Heterostructures With Built-in Electric-Field Effects for High Performance Al-Ion Batteries," *Energy & Environmental Science* 11, no. 11 (2018): 3201–3211.

65. C. Li, S. Dong, P. Wang, C. Wang, and L. Yin, "Metal-Organic Frameworks-Derived Tunnel Structured $Co_3(PO_4)_2$@C as Cathode for New Generation High-Performance Al-Ion Batteries," *Advanced Energy Materials* 9, no. 41 (2019): 1902352.

66. R. Zhuang, G. Miao, Z. Huang, et al., "Non-Stoichiometric $CoS_{1.097}$ Nanoparticles Prepared From CoAl-layered Double Hydroxide and MOF Template as Cathode Materials for Aluminum-Ion Batteries," *Journal of Energy Chemistry* 54 (2021): 639–643.

67. A. Lv, S. Lu, M. Wang, et al., "Self-supporting and Dual-Active 3D Co-S Nanosheets Constructed by Ligand Replacement Reaction From MOF for Rechargeable Al Battery," *Journal of Energy Chemistry* 69 (2022): 35–43.

68. T. Han, H. Bai, J. Xu, et al., "A Metal Organic Framework-Derived Octahedral $Cu_{1.95}S$@CoS_2 for Secondary Batteries Displaying Long Cycle Life and Stable Temperature Tolerance," *Chemical Communications* 59, no. 100 (2023): 14815–14818.

69. H. Bai, J. Xu, J. Liu, T. Han, and J. Niu, "A Nanowire-on-Microrod Polyaniline@FeS_2 Hybrid as the Cathode in High-performance Al-Ion Batteries," *Chemical Communications* 59, no. 75 (2023): 11216–11219.

70. Y. Hu, H. Huang, D. Yu, et al., "All-Climate Aluminum-Ion Batteries Based on Binder-free MOF-derived FeS_2@C/CNT Cathode," *Nanomicro Letters* 13, no. 1 (2021): 159.

71. A. Abouimrane, D. Dambournet, K. W. Chapman, et al., "A New Class of Lithium and Sodium Rechargeable Batteries Based on Selenium and Selenium-Sulfur as a Positive Electrode," *Journal of the American Chemical Society* 134, no. 10 (2012): 4505–4508.

72. C. P. Yang, Y. X. Yin, and Y. G. Guo, "Elemental Selenium for Electrochemical Energy Storage," *Journal of Physical Chemistry Letters* 6, no. 2 (2015): 256–266.

73. X. Chen, L. Peng, L. Wang, et al., "Ether-Compatible Sulfurized Polyacrylonitrile Cathode With Excellent Performance Enabled by Fast Kinetics via Selenium Doping," *Nature Communications* 10, no. 1 (2019): 1021.

74. H. Hong, J. Liu, H. Huang, et al., "Ordered Macro-Microporous Metal-Organic Framework Single Crystals and Theisr Derivatives for Rechargeable Aluminum-Ion Batteries," *Journal of the American Chemical Society* 141, no. 37 (2019): 14764–14771.

75. W. Xing, D. Du, T. Cai, et al., "Carbon-Encapsulated CoSe Nanoparticles Derived From Metal-Organic Frameworks as Advanced Cathode Material for Al-ion Battery," *Journal of Power Sources* 401 (2018): 6–12.

76. G. Wu, W. Lv, X. Li, W. Zhang, and Z. Li, "Metal-Organic Framework Structure With Fe-Co-Se (MIL-88A/Fe-Co@Se) as a Cathode for Aluminum Batteries," *ACS Applied Materials & Interfaces Journal* 13, no. 51 (2021): 61107–61115.

77. J. Li, L. Kang, K. Luo, et al., "Encapsulating Cu_2Se Into 3D Porous Carbon as High-Voltage Electrode Materials for Aluminum-Ion Batteries," *Ceramics International* 49, no. 2 (2023): 2613–2618.

78. B. Zhang, Y. Zhang, J. Li, et al., "In Situ Growth of Metal-Organic Framework-Derived $CoTe_2$ Nanoparticles@Nitrogen-Doped Porous Carbon Polyhedral Composites as Novel Cathodes for Rechargeable Aluminum-Ion Batteries," *Journal of Materials Chemistry A* 8, no. 11 (2020): 5535–5545.

79. T. Qin, L. Qin, and J. Li, "Metal-Organic Framework-Derived CuTe@Porous Carbon Composites as Novel Cathodes for Aluminum Ion Batteries," *Ionics* 28, no. 6 (2022): 2853–2863.

80. H. Bai, K. Tao, Z. Yan, et al., "A Pyramidal Metal-Organic Frameworks-derived FeP@CoP Aluminium-Ion Battery Cathode Displaying Low-temperature Tolerance and Fast Electron Transfer Kinetics," *Chemistry: A European Journal* 29, no. 41 (2023): e202301127.

81. L. Wang, G. Zhu, Y. Lin, et al., "MOF-Derived Hierarchical Porous Carbon Octahedrons for Aluminum-Ion Batteries," *Carbon* 202 (2023): 305–313.

82. S. He, D. Zhang, X. Zhang, et al., "Rechargeable Al-Chalcogen Batteries: Status, Challenges, and Perspectives," *Advanced Energy Materials* 11, no. 29 (2021): 2100769.

83. Q. Pang, J. Meng, S. Gupta, et al., "Fast-Charging Aluminium-Chalcogen Batteries Resistant to Dendritic Shorting," *Nature* 608, no. 7924 (2022): 704–711.

84. Q. Zhou, Y. Wu, J. Gautam, et al., "The Current State of Electrolytes and Cathode Materials Development in the Quest for Aluminum-Sulfur Batteries," *Coordination Chemistry Reviews* 474 (2023): 214856.

85. H. Yang, L. Yin, J. Liang, et al., "An Aluminum-Sulfur Battery With a Fast Kinetic Response," *Angewandte Chemie International Edition* 57, no. 7 (2018): 1898–1902.

86. G. Cohn, L. Ma, and L. A. Archer, "A Novel Non-Aqueous Aluminum Sulfur Battery," *Journal of Power Sources* 283 (2015): 416–422.

87. X. Liu, Y. Li, X. Xu, L. Zhou, and L. Mai, "Rechargeable Metal (Li, Na, Mg, Al)-Sulfur Batteries: Materials and Advances," *Journal of Energy Chemistry* 61 (2021): 104–134.

88. A. E. Baumann, X. Han, M. M. Butala, and V. S. Thoi, "Lithium Thiophosphate Functionalized Zirconium MOFs for Li-S Batteries With Enhanced Rate Capabilities," *Journal of the American Chemical Society* 141, no. 44 (2019): 17891–17899.

89. J. He, Y. Chen, and A. Manthiram, "Vertical Co_9S_8 Hollow Nanowall Arrays Grown on a Celgard Separator as a Multifunctional Polysulfide Barrier for High-performance Li-S Batteries," *Energy & Environmental Science* 11, no. 9 (2018): 2560–2568.

90. Y. Guo, H. Jin, Z. Qi, et al., "Carbonized-MOF as a Sulfur Host for Aluminum-Sulfur Batteries With Enhanced Capacity and Cycling Life," *Advanced Functional Materials* 29, no. 7 (2019): 1807676.

91. X. Xiao, J. Tu, Z. Huang, and S. Jiao, "A Cobalt-Based Metal-Organic Framework and Its Derived Material as Sulfur Hosts for Aluminum-Sulfur Batteries With the Chemical Anchoring Effect," *Physical Chemistry Chemical Physics* 23, no. 17 (2021): 10326–10334.

92. Z. Huang, W. Wang, W. Song, et al., "Electrocatalysis for Continuous Multi-step Reactions in Quasi-Solid-State Electrolytes Towards High-energy and Long-life Aluminum-Sulfur Batteries," *Angewandte Chemie International Edition* 61, no. 24 (2022): e202202696.

93. Z. Huang, S. Li, Z. Wang, et al., "A Hundreds-Milliampere-Hour-Scale Solid-state Aluminum-Sulfur Pouch Cell," *Advanced Energy Materials* 13, no. 43 (2023): 2302464.

94. Q. Zhou, X. Jiang, X. Zhang, et al., "Polyoxomolybdate-Based Metal-Organic Framework-Derived Cu-Embedded Molybdenum Dioxide Hybrid Nanoparticles as Highly Efficient Electrocatalysts for A-S Batteries," *Chemsuschem* 17, no. 19 (2024): e202400424.

95. J. Sun, Z. Du, Y. Liu, et al., "State-of-the-Art and Future Challenges in High Energy Lithium-Selenium Batteries," *Advanced Materials* 33, no. 10 (2021): e2003845.

96. W. Qiu, X. L. Huang, Y. Wang, et al., "Design Strategies of Performance-Enhanced Se Cathodes for Li-Se Batteries and Beyond," *Journal of Energy Chemistry* 76 (2023): 528–546.

97. J. Tu, Z. Huang, C. Chang, et al., "An Efficient Molten-salt Electro-Deoxidation Strategy Enabling Fast-Kinetics and Long-life Aluminum-Selenium Batteries," *SusMat* 4, no. 1 (2024): 126–139.

98. H. Lei, J. Tu, S. Li, et al., "MOF-Based Quasi-Solid-State Electrolyte for Long-life Al-Se Battery," *Journal of Energy Chemistry* 86 (2023): 237–245.

99. S. Jiang, T. Lv, Y. Peng, and H. Pang, "MOFs Containing Solid-State Electrolytes for Batteries," *Advancement of Science* 10, no. 10 (2023): e2206887.

100. Y. He, Y. Qiao, Z. Chang, and H. Zhou, "The Potential of Electrolyte Filled MOF Membranes as Ionic Sieves in Rechargeable Batteries," *Energy & Environmental Science* 12, no. 8 (2019): 2327–2344.

101. S. S. Park, Y. Tulchinsky, and M. Dinca, "Single-Ion Li^+, Na^+, and Mg^{2+} Solid Electrolytes Supported by a Mesoporous Anionic Cu-Azolate Metal-Organic Framework," *Journal of the American Chemical Society* 139, no. 38 (2017): 13260–13263.

102. Z. Huang, W. L. Song, Y. Liu, et al., "Stable Quasi-Solid-State Aluminum Batteries," *Advanced Materials* 34, no. 8 (2022): e2104557.

103. X. Liu, H. Jiao, M. Wang, et al., "Current Progresses and Future Prospects on Aluminium-Air Batteries," *International Materials Reviews* 67, no. 7 (2021): 734–764.

104. Y. Zhang, C. Lv, Y. Zhu, et al., "Challenges and Strategies of Aluminum Anodes for High-performance Aluminum-Air Batteries," *Small Methods* (2023): e2300911.

105. B. Zhu, D. Xia, and R. Zou, "Metal-Organic Frameworks and Their Derivatives as Bifunctional Electrocatalysts," *Coordination Chemistry Reviews* 376 (2018): 430–448.

106. H. T. B. Pham, J. Y. Choi, M. Stodolka, and J. Park, "Maximizing the Potential of Electrically Conductive MOFs," *Accounts of Chemical Research* 57 (2024): 580–589.

107. Y. Liu, Q. Sun, W. Li, et al., "A Comprehensive Review on Recent Progress in Aluminum-Air Batteries," *Green Energy Environ* 2, no. 3 (2017): 246–277.

108. Y. Liu, H. Jiang, J. Hao, et al., "Metal-Organic Framework-Derived Reduced Graphene Oxide-Supported $ZnO/ZnCo_2O_4$/C Hollow Nanocages as Cathode Catalysts for Aluminum-O_2 Batteries," *ACS Applied Materials & Interfaces* 9, no. 37 (2017): 31841–31852.

109. J. Li, N. Zhou, J. Song, et al., "Cu-MOF-Derived Cu/Cu_2O Nanoparticles and CuN_xC_y Species to Boost Oxygen Reduction Activity of Ketjenblack Carbon in Al-Air Battery," *ACS Sustainable Chemistry & Engineering* 6, no. 1 (2017): 413–421.

110. J. Wang, H. Lu, Q. Hong, et al., "Porous N,S-Codoped Carbon Architectures With Bimetallic Sulphide Nanoparticles Encapsulated in Graphitic Layers: Highly Active and Robust Electrocatalysts for the Oxygen Reduction Reaction in Al-Air Batteries," *Chemical Engineering Journal* 330 (2017): 1342–1350.

111. S. Kuppusamy, A. Veedu, A. Mohan, et al., "Punica Grantum Peel Extract Decorated Al-MOF Scaffold as Solid-State Sensor/Concentrator for the Sensing/Reduction of Cr(VI) and Its Extended Utility as a Corrosion Inhibitor in Al-Air Batteries," *Chemical Engineering Journal* 496 (2024): 154070.

112. L. Huang, W. Zang, Y. Ma, et al., "In-Situ Formation of Isolated Iron Sites Coordinated on Nitrogen-Doped Carbon Coated Carbon Cloth as Self-supporting Electrode for Flexible Aluminum-Air Battery," *Chemical Engineering Journal* 421 (2021): 129973.

113. L. Cui, M. Chen, G. Huo, X.-Z. Fu, and J.-L. Luo, "FeCo Nanoparticles Wrapped in N-Doped Carbon Derived From Prussian Blue Analogue and Dicyandiamide as Efficient Oxygen Reduction Electrocatalysts for Al-Air Batteries," *Chemical Engineering Journal* 395 (2020): 125158.

114. R. Mori, "Electrochemical Properties of a Rechargeable Aluminum-Air Battery With a Metal-Organic Framework as Air Cathode Material," *RSC Advances* 7, no. 11 (2017): 6389–6395.

115. S. Zhang, Y. Wang, Y. Li, M. Wei, and K. Wang, "A Polyurethane Organic Framework for Flexible Al-Air Batteries," *ACS Appl Energy Mater* 5, no. 12 (2022): 15909–15917.